Nonlinear aeroservoelastic analysis of a controlled multiple-actuated-wing model with free-play

3 authors, including:

Rui Huang
Nanjing University of Aeronautics & Astronautics
16 PUBLICATIONS **109** CITATIONS

SEE PROFILE

Haiyan Hu
Nanjing University of Aeronautics & Astronautics
219 PUBLICATIONS **3,567** CITATIONS

SEE PROFILE

Nonlinear aeroservoelastic analysis of a controlled multiple-actuated-wing model with free-play

Rui Huang, Haiyan Hu *, Yonghui Zhao

State Key Laboratory of Mechanics and Control of Mechanical Structures, Nanjing University of Aeronautics and Astronautics, 210016 Nanjing, People's Republic of China

ARTICLE INFO

ABSTRACT

In this paper, the effects of structural nonlinearity due to free-play in both leading-edge and trailing-edge outboard control surfaces on the linear flutter control system are analyzed for an aeroelastic model of three-dimensional multiple-actuated-wing. The free-play nonlinearities in the control surfaces are modeled theoretically by using the fictitious mass approach. The nonlinear aeroelastic equations of the presented model can be divided into nine sub-linear modal-based aeroelastic equations according to the different combinations of deflections of the leading-edge and trailing-edge outboard control surfaces. The nonlinear aeroelastic responses can be computed based on these sub-linear aeroelastic systems. To demonstrate the effects of nonlinearity on the linear flutter control system, a single-input and single-output controller and a multi-input and multi-output controller are designed based on the unconstrained optimization techniques. The numerical results indicate that the free-play nonlinearity can lead to either limit cycle oscillations or divergent motions when the linear control system is implemented.

Crown Copyright © 2013 Published by Elsevier Ltd. All rights reserved.

1. Introduction

Nonlinear phenomena in aeroelasticity have been known for many years and have been intensively investigated, e.g., Chen et al. (2011); Cui and Han (2011), Dowell and Tang (2002); Firouz-Abadi et al. (2013); Huang et al. (2012); Marsden and Price (2005); Seo et al. (2011); Stanford and Beran (2013); Vasconcellos et al. (2012), over the past decade or so. Among the studies on nonlinear aeroelasticity, some have dealt with the nonlinear phenomena of the aeroelastic system with the trailing-edge control surface incorporating a structural free-play. For example, Conner et al. (1997) implemented the numerical and experimental study on the nonlinear behavior of a two-dimensional airfoil with a free-play in control surface. Tang et al. (1998) developed a theoretical model for the three-degree-of-freedom aeroelastic system with a free-play via Peters' finite-state model, and studied the Limit Cycle Oscillation (LCO) of the aeroelastic system based on such a theoretical model. Gordon et al. (2008) illustrated the nonlinear stability analysis of control surface flutter with free-play effects based on the describing function method. Those approaches, however, mainly focused on the aeroelastic system in a subsonic flow regime. Dowell et al. (2003) investigated the transonic flutter and the LCO via the airfoil with a free-play in control surface. Jones et al. (2007) used the logarithmic and hyperbolic-tangent functions to reach the accurate approximations to discrete nonlinearities. Coupling these approximations with numerical continuation method, the flutter boundaries and LCOs of the aeroelastic systems with piecewise nonlinear stiffness can be rapidly located with good accuracy.

---

* Corresponding author. Tel.: +86 10 6891 2457; fax: +86 6891 2457.
  E-mail address: hhyae@nuaa.edu.cn (H. Hu).

The above studies have mainly dealt with a kind of simple two-dimensional aeroelastic systems. For three-dimensional aeroelastic system, Shin et al. (2007) showed that the actuator nonlinearities may play an important role in the nonlinear characteristics of an aeroelastic system. However, few studies have focused on the flexible aeroelastic systems with any free-play nonlinearity, such as a three-dimensional wing or an airplane with free-plays in control surfaces, mainly because no general method has been properly established to deal with such a kind of high-dimensional aeroelastic systems.

Karpel and Raveh (1996) proposed a Fictitious Mass (FM) approach to improve the accuracy and efficiency of the modal-based structural analysis that involves substructure synthesis, location excitation and local structural changes. The FM approach has provided an accurate and efficient method to deal with a high-dimensional aeroelastic system with free-plays (Bae et al., 2004; Lee and Kim, 1995; Kim et al., 2008; Lee and Chen, 2006). Bae et al. (2002) investigated the linear and nonlinear aeroelastic behaviors of a fighter-type wing with a control surface. They established the mathematical model of an aeroelastic system via the FM approach, and implemented the linear and nonlinear analyses via the frequency domain method and time-integration, respectively. The numerical results in this paper showed the LCOs observed for a wide range of flow speeds below the linear flutter boundary. Gold and Karpel (2008) developed the aeroservoelastic equations of reduced-size and implemented the stability analysis and maneuver simulation of a control-augmented uninhabited aerial vehicle (UAV) with the actuator nonlinearity caused by the free-play in control surface.

The above mentioned studies, however, have only dealt with the nonlinear aeroelastic or aeroservoelastic analyses, and have not yet touched with the effects of the structural nonlinearities on an aeroservoelastic system. Dimitriadis and Cooper (2000) studied the stability of a simple aeroservoelastic system with nonlinearities in the control system and power control unit. Their numerical results demonstrated that the simple feedback systems designed to increase the stability of the linearized system also stabilize the nonlinear system although their effects can be less pronounced. Frampton and Clark (2000) designed a linear LQG controller to reduce or eliminate the LCO in a typical airfoil section with a free-play in the flap restoring stiffness, but made the controller design based on a linear aeroelastic system without any free-play. Their experimental results demonstrated that the control system was effective to eliminate the LCO for the studied model. Later on, Bae (2002) performed the study on the flutter suppression of a wing with a free-play by using the linear LQG controller and the sliding mode controller (SMC). However, he illustrated that the linear LQG controller might not suppress or reduce the LCOs of the wing with a free-play and the SMC has better performance to suppress LCOs. Hence, some question naturally arises. For example, one may wonder whether similar results are available when the linear control law is implemented on a three-dimensional aeroelastic system with multiple free-plays in the Leading-Edge Outboard (LEO) and Trailing-Edge Outboard (TEO) control surfaces. Moreover, the design objective of the advanced flutter suppression laws is to develop a low-order robust Multi-Input and Multi-Output (MIMO) control law. Therefore, one may ask whether the MIMO controller can still be effective if all of the control surfaces have free-plays. Thus, an important issue that needs to be addressed is to gain an insight into the effects of free-plays on the linear control systems (either SISO or MIMO) of a three-dimensional aeroelastic system.

The objective of this study is to reveal the nonlinear effects of free-plays in the control surfaces on the linear flutter suppression system. The paper is organized as follows. In Section 2, the FM approach is introduced, and the linear flutter analysis based on the FM approach and the analysis based on the direct approach are compared via a three-dimensional multiple-actuated-wing model. In Section 3, the open-loop aeroelastic equations of an aeroelastic system with free-plays in both LEO and TEO control surfaces are established via the FM approach. In Section 4, two reduce-ordered optimal linear control laws, the MIMO law and the SISO law, are designed based on the nominal linear aeroelastic system without any free-play. In Section 5, an illustrative example is given to demonstrate the nonlinear effects of the free-plays in control surfaces on the open-loop and closed-loop aeroelastic systems. Finally, a few concluding remarks are made in Section 6.
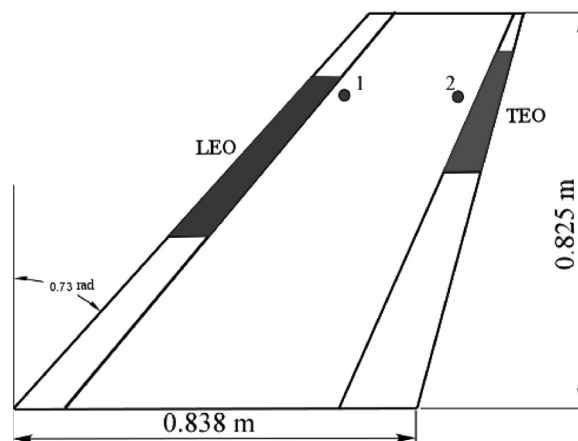

Fig. 1. Configuration of the MAW model, where the numbers 1 and 2 indicate the sensor locations and the shaded control surfaces are used for flutter suppression.

2. FM approach and linear flutter analysis

The evaluation of the effects of free-plays in both LEO and TEO control surfaces on the aeroelastic and aeroservoelastic responses is important for the design of flight vehicles. Such an evaluation enables one to investigate the structural changes during the dynamic response. For example, when the LEO and/or TEO control surfaces pass through the free-play zone, the structural properties of the aeroelastic/aeroservoelastic model are subject to a change. The conventional aeroelastic analysis starts with the computation of a limit set of low-frequency normal modes, which serve as the generalized coordinates for further studies. However, the repeated computation of normal modes and the associated generalized aerodynamic forces when a structural property changes is often impractical. In addition, it is complicated to deal with the changing coordinates during the dynamic analysis in time-domain analysis. These problems can be solved by performing the entire analysis with a constant set of modal coordinates. Using this constant set of modal coordinates, when the LEO and/or TEO control surfaces pass into or exit from the free-play zones, all the structural properties can be represented. These constant modal coordinates can be obtained via the FM approach (Karpel and Raveh, 1996). In this approach, a large FM is added to some degrees of freedom, where the structural changes will occur. The basic idea of the approach is that the effects of large structural variations can be properly accounted for only when the modes that serve as generalized coordinates contain significant distortions in the vicinity of the varying structural elements. This section introduces the FM approach and implements the linear flutter analysis of the wind-tunnel model of a Multiple-Actuated Wing (MAW), as shown in Fig. 1, based on the FM approach. The MAW model includes two control surfaces driven by rotary servo motors used to suppress possible flutters. The nonlinearity of the MAW model is due to the free-play in the actuator when the aileron hinge moment changes its sign. For most of the control surfaces, the free-play bounds for the ailerons and flaperons are 0.13° and 0.57°, respectively (Anderson and Mortara, 2007). In this work, both LEO and TEO control surfaces are assumed to have the same free-play angle, $\delta_f = 0.5°$.

2.1. FM approach

The FM approach provides an accurate treatment of structural nonlinearities, such as the free-play in a control surface. For the finite element approach, the control surface is connected to the wing structure by a rotational spring. The free-play of the control surface actuator can be represented by changing the actuator stiffness from its nominal value to zero during the simulation while the control surface angle falls into the free-play zone. In the following numerical example, the use of two fictitious masses at the LEO and TEO rotational springs provides a convenient way to evaluate the actuator behavior while the control surfaces travel into and leave from the free-play zone. To demonstrate the FM model, a set of 20 normal modes is generated by using MSC/NASTRAN with both LEO and TEO springs assigned a soft stiffness actuator value of $k_\alpha = 0.0$ Nm/rad and loaded with two large fictitious moments of inertia, 1200 kg·m² and 50 kg·m², respectively. The modal shapes Φ_f and corresponding generalized coordinates ξ_f of the FM model can serve as a constant set of generalized coordinates of the structure throughout the dynamic analysis. To verify that the FM modes do not change the characteristics of the four sub-linear structures, the natural frequencies are compared with those computed by using the direct method in MSC/NASTRAN and the indirect method with the FM approach. The dynamic equations of the four sub-linear models are

Table 1
Computed modes of the wing with LEO and/or TEO free-plays compared with the FM results.

Mode	FM included, Hz	LEO free-play		TEO free-play		LEO and TEO free-plays		Without free-play	
		Direct model	FM model	Direct model	FM model	Direct method	FM approach	Direct model	FM approach
1	0	0.0189	0.0189	0.0819	0.0819	0.0189	0.0189	3.2961	3.2961
2	0	3.3201	3.3201	3.2983	3.2983	0.0819	0.0819	9.4171	9.4203
3	3.2946	9.8511	9.8522	9.4259	9.4291	3.3223	3.3223	12.8177	12.8182
4	9.4778	12.8578	12.8580	12.8234	12.8239	9.8611	9.8621	13.9155	13.9155
5	12.8226	13.9155	13.9155	13.9155	13.9155	12.8626	12.8628	19.4322	19.4502
6	13.9155	19.8773	19.8782	19.4333	19.4512	13.9155	13.9155	25.5446	25.5890
7	19.7946	26.0636	26.0641	25.5453	25.5895	19.8779	19.8788	32.1520	32.1626
8	26.0273	32.1692	32.1708	32.1912	32.2003	26.0638	26.0643	32.8934	33.4628
9	32.0385	37.2330	37.2331	32.8982	33.4685	32.2048	32.2067	37.2330	37.2331
10	34.5051	38.1091	38.2177	37.2331	37.2331	37.2331	37.2331	42.2690	42.4349
11	37.2331	42.8830	42.9254	42.2723	42.4361	38.1291	38.2367	44.4161	45.1689
12	42.0899	48.6553	48.7479	44.4354	45.1905	42.8843	42.9266	49.3646	49.6475
13	46.6796	55.0352	55.0352	49.3721	49.6529	48.6690	48.7629	55.0352	55.0352
14	52.0690	55.5718	55.5981	55.0352	55.0352	55.0352	55.0352	55.5736	55.6081
15	55.0352	60.5238	61.2176	55.7119	55.7422	55.7098	55.7323	61.7652	61.7657
16	55.8716	61.7657	61.7657	61.7657	61.7657	60.5305	61.2249	62.7371	62.8615
17	61.7657	64.7896	67.2292	62.7492	62.8759	61.7657	61.7657	69.4646	69.9256
18	62.3641	71.1138	71.7099	69.4804	69.9379	64.7917	67.2333	73.5054	76.1548
19	70.5061	73.5054	87.3645	73.5054	76.1961	71.1267	71.7584	73.8956	146.9106
20	73.3836	73.9890	470.9049	73.9817	146.9113	73.5054	87.3739	76.5446	470.9050

given as

$$(\Phi_f^T \mathbf{M}_{NM} \Phi_f)\ddot{\xi}_f + (\Phi_f^T \mathbf{K}_{NM} \Phi_f)\xi_f = 0, \tag{1}$$

$$(\Phi_f^T \mathbf{M}_{NM} \Phi_f)\ddot{\xi}_f + (\Phi_f^T \mathbf{K}_L \Phi_f)\xi_f = 0, \tag{2}$$

$$(\Phi_f^T \mathbf{M}_{NM} \Phi_f)\ddot{\xi}_f + (\Phi_f^T \mathbf{K}_T \Phi_f)\xi_f = 0, \tag{3}$$

$$(\Phi_f^T \mathbf{M}_{NM} \Phi_f)\ddot{\xi}_f + (\Phi_f^T \mathbf{K}_{LT} \Phi_f)\xi_f = 0, \tag{4}$$

where $\mathbf{M}_{NM}$, $\mathbf{K}_{NM}$, $\mathbf{K}_L$, $\mathbf{K}_T$ and $\mathbf{K}_{LT}$ are the full discrete-coordinate mass and stiffness matrices of the structural model without any free-play, with an LEO free-play, with a TEO free-play and with both LEO and TEO free-plays, respectively. In Table 1, the natural frequencies computed via the FM approach agree well with those obtained via the direct method except for a few of very high frequencies. It should be noted that those modes of very high frequencies computed via the FM approach reflect some local vibrations, instead of any natural modes. However, they are included to account for the local vibrations in subsequent analyses. Fig. 2 shows four dominant natural modes of the MAW model with the fixed hinge stiffness, i.e., $k_\alpha = 30$ Nm/rad, computed via the FM approach. The figure does not show the fourth in-plane mode because it contributes much less to the wing flutter. The high accuracy, demonstrated in Table 1 and Fig. 2, proves that the use of FM modal coordinates provides an accurate treatment of the actuator nonlinearity in modal-based analysis with large actuator stiffness change.

2.2. Linear flutter analysis via the FM approach

To further validate the FM approach, a linear flutter analysis of the four sub-linear structures is implemented individually by using the FM and direct methods. In this study, the structural damping of the MAW model is not taken into consideration for simplicity. The direct flutter solution of each sub-linear structure is determined with the modal parameters of the corresponding sub-linear structure. The modal parameters of each sub-linear structure can be obtained via the free-vibration solution of the corresponding FEM model. For the FM approach, the dynamic equations in the flutter analysis of the four sub-linear structures are given as

$$\left[\frac{V^2}{b^2} \mathbf{M}_{HH} p^2 + \mathbf{K}_{HH} - q_d \mathbf{Q}_{HH}(p) \right] \xi_f = \mathbf{0}, \tag{5}$$

The first mode (bending), 3.2961 Hz   The second model (torsion), 9.4203 Hz

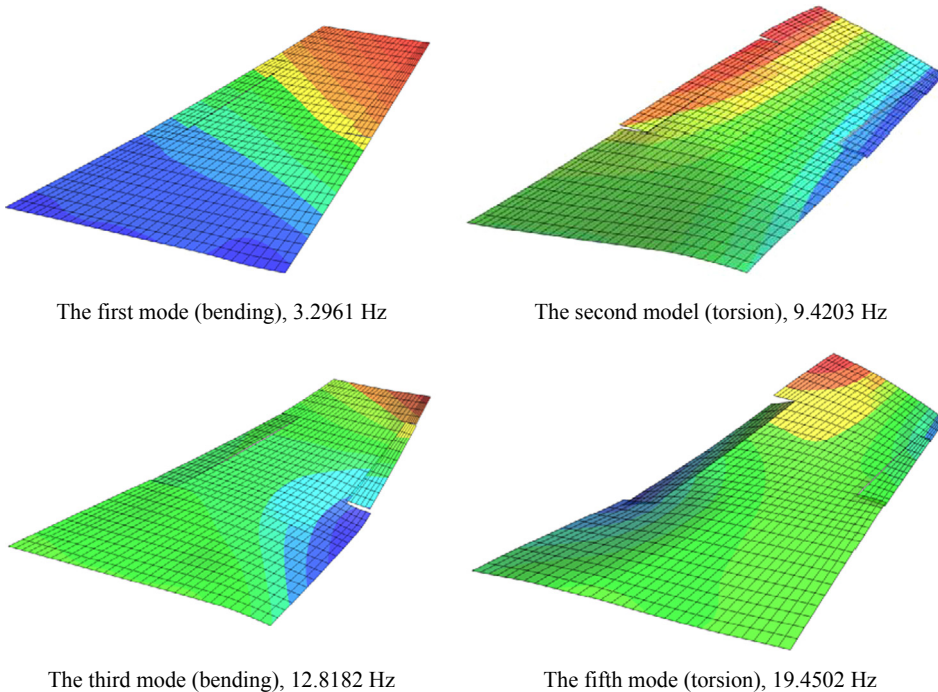The third mode (bending), 12.8182 Hz   The fifth mode (torsion), 19.4502 Hz

Fig. 2. Four dominant natural modes of the MAW model with hinge stiffness $k_\alpha = 30$ Nm/rad computed by using the FM approach.

$$\left[\frac{V^2}{b^2}\mathbf{M}_{\mathrm{HH}}p^2 + \mathbf{K}_{\mathrm{HHL}} - q_{\mathrm{d}}\mathbf{Q}_{\mathrm{HH}}(p)\right]\xi_{\mathrm{f}} = \mathbf{0}, \tag{6}$$

$$\left[\frac{V^2}{b^2}\mathbf{M}_{\mathrm{HH}}p^2 + \mathbf{K}_{\mathrm{HHT}} - q_{\mathrm{d}}\mathbf{Q}_{\mathrm{HH}}(p)\right]\xi_{\mathrm{f}} = \mathbf{0}, \tag{7}$$

$$\left[\frac{V^2}{b^2}\mathbf{M}_{\mathrm{HH}}p^2 + \mathbf{K}_{\mathrm{HHLT}} - q_{\mathrm{d}}\mathbf{Q}_{\mathrm{HH}}(p)\right]\xi_{\mathrm{f}} = \mathbf{0}, \tag{8}$$

where q_{d}, V and b are the dynamic pressure, flight speed and semi-chord, respectively. The generalized mass and stiffness matrices $\mathbf{M}_{\mathrm{HH}}$ $\mathbf{K}_{\mathrm{HH}}$,$\mathbf{K}_{\mathrm{HHL}}$,$\mathbf{K}_{\mathrm{HHT}}$ and $\mathbf{K}_{\mathrm{HHLT}}$ are obtained as follows:

$$\mathbf{M}_{\mathrm{HH}} = \Phi_{\mathrm{f}}^{\mathrm{T}}\mathbf{M}_{\mathrm{NM}}\Phi_{\mathrm{f}}, \quad \mathbf{K}_{\mathrm{HH}} = \Phi_{\mathrm{f}}^{\mathrm{T}}\mathbf{K}_{\mathrm{NM}}\Phi_{\mathrm{f}}, \quad \mathbf{K}_{\mathrm{HHL}} = \Phi_{\mathrm{f}}^{\mathrm{T}}\mathbf{K}_{\mathrm{L}}\Phi_{\mathrm{f}}, \quad \mathbf{K}_{\mathrm{HHT}} = \Phi_{\mathrm{f}}^{\mathrm{T}}\mathbf{K}_{\mathrm{T}}\Phi_{\mathrm{f}}, \quad \mathbf{K}_{\mathrm{HHLT}} = \Phi_{\mathrm{f}}^{\mathrm{T}}\mathbf{K}_{\mathrm{LT}}\Phi_{\mathrm{f}} \tag{9}$$

In this study, the generalized aerodynamic forces $\mathbf{Q}_{\mathrm{HH}}(p)$ involving the elastic modes are computed via the doublet-lattice method (Albano and Rodden, 1969). The comparison of the flutter speed and frequency between the FM approach and the direct method of the four sub-linear structures is shown in Table 2. The direct method for flutter solutions is implemented by using the aeroelastic module of MSC NASTRAN. The high-level of agreement between the results of two methods shows that the FM modes, when used for the nonlinear flutter analysis of the MAW model with two free-plays, can accurately represent the physical deformation in the entire domain of the nonlinear dynamic response.

Table 2
Comparison of the flutter solutions of the four sub-linear structures by using the FM approach and the direct method.

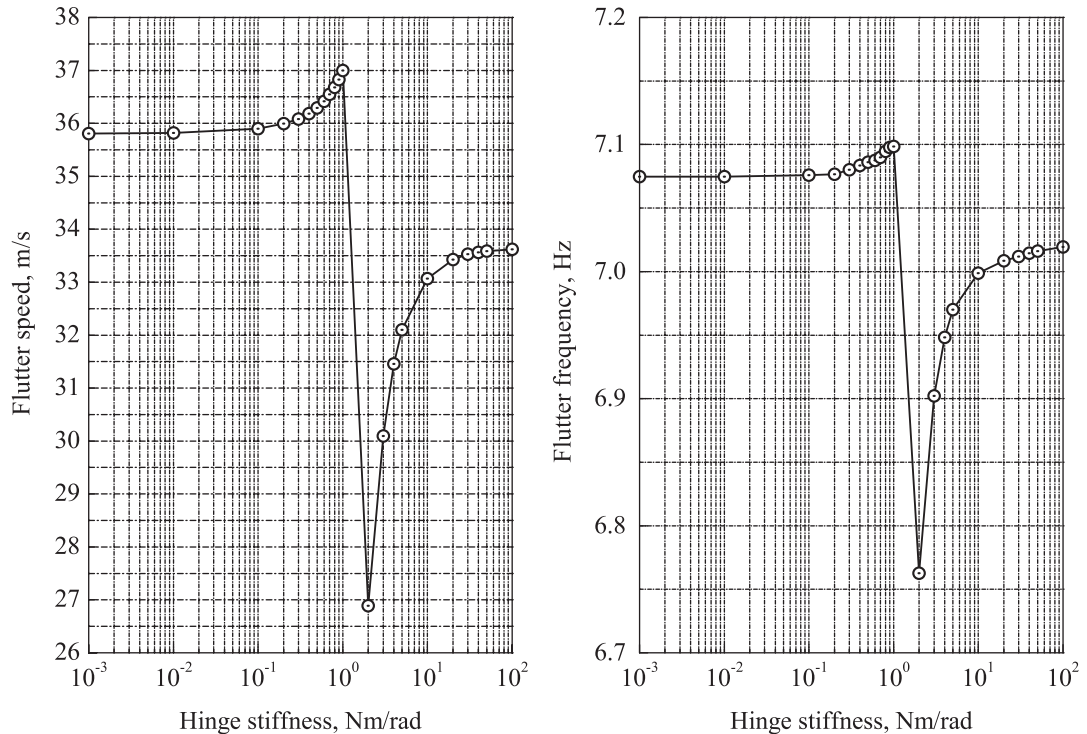| Sub-system	Nominal		LEO free-play		TEO free-play		Both free-plays	
Method	Direct method	FM approach	Direct method	FM approach	Direct method	FM approach	Direct method	FM approach
Flutter speed (m/s)	33.5270	33.4919	35.8080	35.776	31.479	31.4932	33.882	33.878
Flutter Freq. (Hz)	7.0117	7.0248	7.0746	7.0806	7.3848	7.3886	7.4623	7.4628

Fig. 3. Flutter speed and frequency with the variation of LEO hinge stiffness.
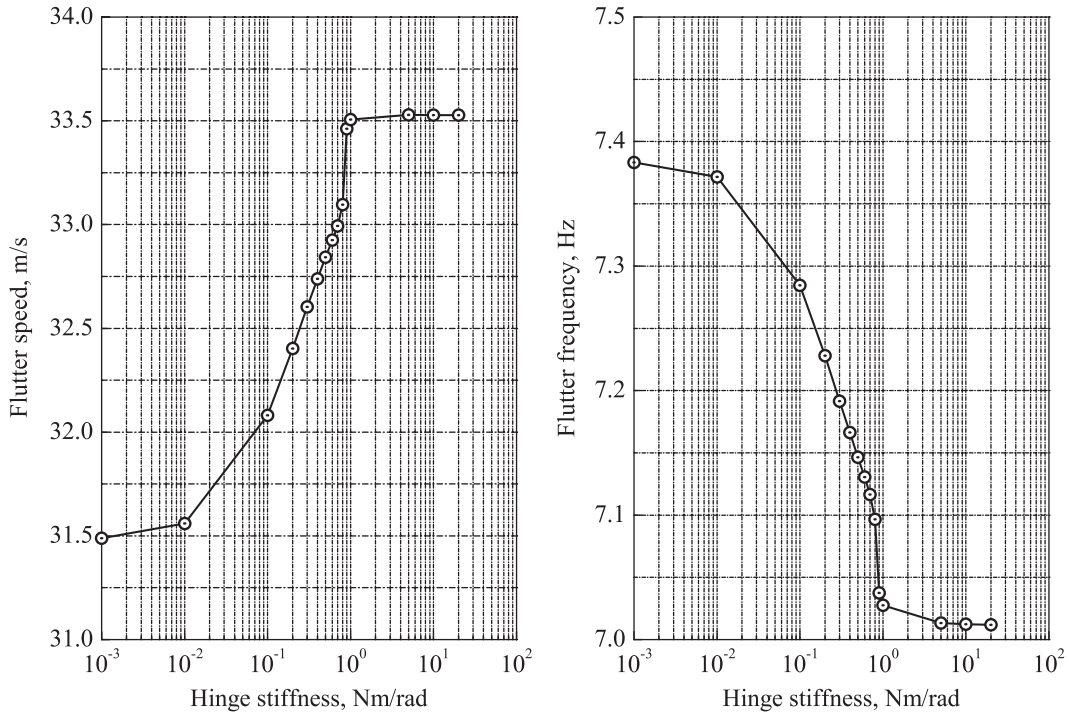
Fig. 4. Flutter speed and frequency with the variation of TEO hinge stiffness.

Figs. 3 and 4 show the flutter speeds and frequencies with the variation of the LEO and TEO hinge stiffness values, respectively. To investigate the effect of the LEO hinge stiffness on the aeroelastic characteristics of the MAW model, the TEO hinge stiffness is set to be a constant, i.e., 30 Nm/rad. Fig. 3 shows the jump in the flutter speed and frequency of the MAW model with LEO and TEO control surfaces. This jump is due to a sudden transition between two flutter modes. Moreover, the phenomenon of low-speed static divergence appears when the MAW model involves a small LEO hinge stiffness value, such as 0.01 Nm/rad. Fig. 4 shows the effect of TEO hinge stiffness on the aeroelastic characteristics of the MAW model when the LEO hinge stiffness is set to be 30 Nm/rad. The flutter characteristic in Fig. 4 can be subdivided into two regions. The first is the bending-torsional-flapping mode coalescent flutter when the TEO actuator involves the hinge stiffness smaller than 0.1 Nm/rad. The second is the bending-torsional mode (first bending-first torsion mode) coalescent flutter when the TEO hinge stiffness is larger than 0.1 Nm/rad. These two figures also show that the flutter characteristics are similar to that of a clean wing when both LEO and TEO hinge stiffness values are larger than 30 Nm/rad.

3. Nonlinear aeroelastic analysis of the MAW model with free-plays

The procedure of establishing the nonlinear aeroelastic equations of the MAW model with free-plays can be divided into two steps. At first, the dynamic equations of the system are established in the physical space. Then, they are obtained in modal coordinates via the FM approach. Once the nonlinear aeroelastic equations are established for the MAW model with free-plays, several numerical methods have been available for analyzing the nonlinear dynamics of the aeroelastic system. Among them, the time-integration method (Conner et al., 1997) and the describing function method (Tang et al. 1998) are relatively simple. To get the more accurate periodic response or the related bifurcation diagram, Liu et al. (2002) and Chung et al. (2007) developed the point transformation (PT) method and perturbation-incremental (PI) method to analyze the nonlinear dynamics of a two-dimensional aeroelastic system with free-play models, respectively. Compared with the time-integration method, the PT method can precisely locate the state transition between two linear regions of the piecewise linear system. Prior to the PT method, the PI method is suitable for performing the parametric continuation of a periodic response. For simplicity, the time-integration method is used in this study to solve the nonlinear aeroservoelastic equations of the MAW model with free-plays in both LEO and TEO control surfaces. To reduce the numerical error caused by the inexact location of a state transition between two linear regions, the time step is set to be a very fine value, say, $\Delta t = 10^{-3}$ s.

3.1. Aeroelastic equations with free-plays

The dynamic equation of the aeroelastic system with concentrated structural nonlinearities can be written as follows:

$$\mathbf{M}\ddot{\mathbf{u}} + \mathbf{C}\dot{\mathbf{u}} + \mathbf{R}(\mathbf{u}) - \mathbf{F}_a = \mathbf{F}_g, \tag{10}$$

where $\mathbf{R}(\mathbf{u})$, $\mathbf{F}_a$ and $\mathbf{F}_g$ are the nonlinear elastic restoring force vector, unsteady aerodynamic forces and external gust loads, respectively. For the nonlinearity of a free-play, the restoring force vector can be written as follows:

$$\mathbf{R}(\mathbf{u}) = \mathbf{K}\mathbf{u} + \mathbf{P}\{f(\theta_s)\}, \tag{11}$$

where $\mathbf{K}$ is the linear stiffness matrix without any free-play, $f(\theta_s)$ is the restoring force and $\mathbf{P}(6 \times n, 2)$ is the chosen matrix whose entries are zero except for the nonlinear elements. Here, n is the grid number of the structural model. More specifically, the single restoring force can be described as follows:

$$f(\theta_s) = \begin{cases} 0, & |\theta_s| \le \delta_f, \\ K_\theta(\theta_s - \delta_f), & |\theta_s| > \delta_f. \end{cases} \tag{12}$$

By combining Eqs. (10), (11) and (12), one obtains the dynamic equations of the MAW model with free-plays in both LEO and TEO control surfaces as follows:

For $\theta_{LEO} > \delta_{LEO}$ and $\theta_{TEO} > \delta_{TEO}$

$$\mathbf{M}\ddot{\mathbf{u}} + \mathbf{C}\dot{\mathbf{u}} + \left(\mathbf{K} + \mathbf{P}\begin{bmatrix} K_{LEO} & 0 \\ 0 & K_{TEO} \end{bmatrix}\mathbf{P}^T\right)\mathbf{u} - \mathbf{F}_a = \mathbf{F}_g + \left(\mathbf{P}\begin{bmatrix} K_{LEO} & 0 \\ 0 & K_{TEO} \end{bmatrix}\mathbf{P}^T\right)\{\delta_{1p2}\}, \tag{13}$$

For $\theta_{LEO} < -\delta_{LEO}$ and $\theta_{TEO} < -\delta_{TEO}$

$$\mathbf{M}\ddot{\mathbf{u}} + \mathbf{C}\dot{\mathbf{u}} + \left(\mathbf{K} + \mathbf{P}\begin{bmatrix} K_{LEO} & 0 \\ 0 & K_{TEO} \end{bmatrix}\mathbf{P}^T\right)\mathbf{u} - \mathbf{F}_a = \mathbf{F}_g - \left(\mathbf{P}\begin{bmatrix} K_{LEO} & 0 \\ 0 & K_{TEO} \end{bmatrix}\mathbf{P}^T\right)\{\delta_{1p2}\}, \tag{14}$$

For $\theta_{LEO} > \delta_{LEO}$ and $\theta_{TEO} < -\delta_{TEO}$

$$\mathbf{M}\ddot{\mathbf{u}} + \mathbf{C}\dot{\mathbf{u}} + \left(\mathbf{K} + \mathbf{P}\begin{bmatrix} K_{LEO} & 0 \\ 0 & K_{TEO} \end{bmatrix}\mathbf{P}^T\right)\mathbf{u} - \mathbf{F}_a = \mathbf{F}_g + \left(\mathbf{P}\begin{bmatrix} K_{LEO} & 0 \\ 0 & K_{TEO} \end{bmatrix}\mathbf{P}^T\right)\{\delta_{1m2}\}, \tag{15}$$

For $\theta_{LEO} < -\delta_{LEO}$ and $\theta_{TEO} > \delta_{TEO}$

$$\mathbf{M}\ddot{\mathbf{u}} + \mathbf{C}\dot{\mathbf{u}} + \left(\mathbf{K} + \mathbf{P}\begin{bmatrix} K_{LEO} & 0 \\ 0 & K_{TEO} \end{bmatrix}\mathbf{P}^T\right)\mathbf{u} - \mathbf{F}_a = \mathbf{F}_g - \left(\mathbf{P}\begin{bmatrix} K_{LEO} & 0 \\ 0 & K_{TEO} \end{bmatrix}\mathbf{P}^T\right)\{\delta_{1m2}\}, \tag{16}$$

For $\theta_{LEO} > \delta_{LEO}$ and $-\delta_{TEO} \le \theta_{TEO} \le \delta_{TEO}$

$$\mathbf{M}\ddot{\mathbf{u}} + \mathbf{C}\dot{\mathbf{u}} + \left(\mathbf{K} + \mathbf{P}\begin{bmatrix} K_{LEO} & 0 \\ 0 & 0 \end{bmatrix}\mathbf{P}^T\right)\mathbf{u} - \mathbf{F}_a = \mathbf{F}_g + \left(\mathbf{P}\begin{bmatrix} K_{LEO} & 0 \\ 0 & 0 \end{bmatrix}\mathbf{P}^T\right)\{\delta_{LEO}\}, \tag{17}$$

For $\theta_{LEO} < -\delta_{LEO}$ and $-\delta_{TEO} \le \theta_{TEO} \le \delta_{TEO}$

$$\mathbf{M}\ddot{\mathbf{u}} + \mathbf{C}\dot{\mathbf{u}} + \left(\mathbf{K} + \mathbf{P}\begin{bmatrix} K_{LEO} & 0 \\ 0 & 0 \end{bmatrix}\mathbf{P}^T\right)\mathbf{u} - \mathbf{F}_a = \mathbf{F}_g - \left(\mathbf{P}\begin{bmatrix} K_{LEO} & 0 \\ 0 & 0 \end{bmatrix}\mathbf{P}^T\right)\{\delta_{LEO}\}, \tag{18}$$

For $-\delta_{LEO} \le \theta_{LEO} \le \delta_{LEO}$ and $\theta_{TEO} > \delta_{TEO}$

$$\mathbf{M}\ddot{\mathbf{u}} + \mathbf{C}\dot{\mathbf{u}} + \left(\mathbf{K} + \mathbf{P}\begin{bmatrix} 0 & 0 \\ 0 & K_{TEO} \end{bmatrix}\mathbf{P}^T\right)\mathbf{u} - \mathbf{F}_a = \mathbf{F}_g + \left(\mathbf{P}\begin{bmatrix} 0 & 0 \\ 0 & K_{TEO} \end{bmatrix}\mathbf{P}^T\right)\{\delta_{TEO}\}, \tag{19}$$

For $-\delta_{LEO} \le \theta_{LEO} \le \delta_{LEO}$ and $\theta_{TEO} < -\delta_{TEO}$

$$\mathbf{M}\ddot{\mathbf{u}} + \mathbf{C}\dot{\mathbf{u}} + \left(\mathbf{K} + \mathbf{P}\begin{bmatrix} 0 & 0 \\ 0 & K_{TEO} \end{bmatrix}\mathbf{P}^T\right)\mathbf{u} - \mathbf{F}_a = \mathbf{F}_g - \left(\mathbf{P}\begin{bmatrix} 0 & 0 \\ 0 & K_{TEO} \end{bmatrix}\mathbf{P}^T\right)\{\delta_{TEO}\}, \tag{20}$$

For $-\delta_{LEO} \le \theta_{LEO} \le \delta_{LEO}$ and $-\delta_{TEO} \le \theta_{TEO} \le \delta_{TEO}$

$$\mathbf{M}\ddot{\mathbf{u}} + \mathbf{C}\dot{\mathbf{u}} + \mathbf{K}\mathbf{u} - \mathbf{F}_a = \mathbf{F}_g, \tag{21}$$

where $\theta_{LEO}, \delta_{LEO}, \theta_{TEO}, \delta_{TEO}$ are the deflections and free-play angles of the LEO and TEO control surfaces. K_{LEO} and K_{TEO} are the stiffness coefficients of the LEO and TEO rotational springs, respectively. The positive directions of deflections θ_{LEO} and θ_{TEO} of the LEO and TEO control surfaces are defined as up and down, respectively. $\{\delta_{1p2}\}$ and $\{\delta_{1m2}\}$ can be computed as follows:

$$\{\delta_{1p2}\} = \{\delta_{LEO}\} + \{\delta_{TEO}\}, \quad \{\delta_{1m2}\} = \{\delta_{LEO}\} - \{\delta_{TEO}\}. \tag{22}$$

With the help of the FM approach, the total nine sub-linear aeroelastic Eqs. (13), ((14)–(21) can be rewritten in the modal coordinates as follows:

$$\mathbf{M}_{HH}\ddot{\xi}_f + \mathbf{C}_{HH}\dot{\xi}_f + \mathbf{K}_{HH}\xi_f - q_d\begin{bmatrix} \mathbf{Q}_{HH} & \mathbf{Q}_{HC} \end{bmatrix}\begin{Bmatrix} \xi_f \\ \delta^c_{LEO} \\ \delta^c_{TEO} \end{Bmatrix} = -\frac{q_d}{V}\mathbf{Q}_{HG}(ik)w_G(ik) + \mathbf{\Phi}_f^T[\mathbf{K}_{NM} - \mathbf{K}_{LT}]\{\delta_{1p2}\}, \tag{23}$$

$$\mathbf{M}_{HH}\ddot{\xi}_f + \mathbf{C}_{HH}\dot{\xi}_f + \mathbf{K}_{HH}\xi_f - q_d\left[\mathbf{Q}_{HH} \quad \mathbf{Q}_{HC}\right]\left\{\begin{array}{c}\xi_f \\ \delta^c_{LEO} \\ \delta^c_{TEO}\end{array}\right\} = -\frac{q_d}{V}\mathbf{Q}_{HG}(ik)w_G(ik) - \mathbf{\Phi}^T_f[\mathbf{K}_{NM} - \mathbf{K}_{LT}]\{\delta_{1p2}\},\tag{24}$$

$$\mathbf{M}_{HH}\ddot{\xi}_f + \mathbf{C}_{HH}\dot{\xi}_f + \mathbf{K}_{HH}\xi_f - q_d\left[\mathbf{Q}_{HH} \quad \mathbf{Q}_{HC}\right]\left\{\begin{array}{c}\xi_f \\ \delta^c_{LEO} \\ \delta^c_{TEO}\end{array}\right\} = -\frac{q_d}{V}\mathbf{Q}_{HG}(ik)w_G(ik) + \mathbf{\Phi}^T_f[\mathbf{K}_{NM} - \mathbf{K}_{LT}]\{\delta_{1m2}\},\tag{25}$$

$$\mathbf{M}_{HH}\ddot{\xi}_f + \mathbf{C}_{HH}\dot{\xi}_f + \mathbf{K}_{HH}\xi_f - q_d\left[\mathbf{Q}_{HH} \quad \mathbf{Q}_{HC}\right]\left\{\begin{array}{c}\xi_f \\ \delta^c_{LEO} \\ \delta^c_{TEO}\end{array}\right\} = -\frac{q_d}{V}\mathbf{Q}_{HG}(ik)w_G(ik) - \mathbf{\Phi}^T_f[\mathbf{K}_{NM} - \mathbf{K}_{LT}]\{\delta_{1m2}\},\tag{26}$$

$$\mathbf{M}_{HH}\ddot{\xi}_f + \mathbf{C}_{HH}\dot{\xi}_f + \mathbf{K}_{HHT}\xi_f - q_d\left[\mathbf{Q}_{HH} \quad \mathbf{Q}_{HC}\right]\left\{\begin{array}{c}\xi_f \\ \delta^c_{LEO} \\ 0\end{array}\right\} = -\frac{q_d}{V}\mathbf{Q}_{HG}(ik)w_G(ik) + \mathbf{\Phi}^T_f[\mathbf{K}_{NM} - \mathbf{K}_{L}]\{\delta_{LEO}\},\tag{27}$$

$$\mathbf{M}_{HH}\ddot{\xi}_f + \mathbf{C}_{HH}\dot{\xi}_f + \mathbf{K}_{HHT}\xi_f - q_d\left[\mathbf{Q}_{HH} \quad \mathbf{Q}_{HC}\right]\left\{\begin{array}{c}\xi_f \\ \delta^c_{LEO} \\ 0\end{array}\right\} = -\frac{q_d}{V}\mathbf{Q}_{HG}(ik)w_G(ik) - \mathbf{\Phi}^T_f[\mathbf{K}_{NM} - \mathbf{K}_{L}]\{\delta_{LEO}\},\tag{28}$$

$$\mathbf{M}_{HH}\ddot{\xi}_f + \mathbf{C}_{HH}\dot{\xi}_f + \mathbf{K}_{HHL}\xi_f - q_d\left[\mathbf{Q}_{HH} \quad \mathbf{Q}_{HC}\right]\left\{\begin{array}{c}\xi_f \\ 0 \\ \delta^c_{TEO}\end{array}\right\} = -\frac{q_d}{V}\mathbf{Q}_{HG}(ik)w_G(ik) + \mathbf{\Phi}^T_f[\mathbf{K}_{NM} - \mathbf{K}_{T}]\{\delta_{TEO}\},\tag{29}$$

$$\mathbf{M}_{HH}\ddot{\xi}_f + \mathbf{C}_{HH}\dot{\xi}_f + \mathbf{K}_{HHL}\xi_f - q_d\left[\mathbf{Q}_{HH} \quad \mathbf{Q}_{HC}\right]\left\{\begin{array}{c}\xi_f \\ 0 \\ \delta^c_{TEO}\end{array}\right\} = -\frac{q_d}{V}\mathbf{Q}_{HG}(ik)w_G(ik) - \mathbf{\Phi}^T_f[\mathbf{K}_{NM} - \mathbf{K}_{T}]\{\delta_{TEO}\},\tag{30}$$

$$\mathbf{M}_{HH}\ddot{\xi}_f + \mathbf{C}_{HH}\dot{\xi}_f + \mathbf{K}_{HHLT}\xi_f + q_d\mathbf{Q}_{HH}(ik)\xi_f = -\frac{q_d}{V}\mathbf{Q}_{HG}(ik)w_G(ik),\tag{31}$$

where $\mathbf{Q}_{HC}, \delta^c_{LEO}, \delta^c_{TEO}$ and k are the generalized aerodynamic forces between the elastic modes and control modes, the deflections of the LEO and TEO control surfaces and the reduced frequency, respectively. Eqs. (23)–(31) illustrate that the variations of structural property can be represented by a constant set of fictitious modes, and the generalized aerodynamic forces only need to be computed based on the fictitious modes. Thus, there is no need to compute the normal modes and aerodynamic forces repeatedly when any structural property of the aeroelastic/aeroservoelastic model is changed. Moreover, there is no need to deal with the change of coordinates during the dynamic analysis in time domain because the nine sub-linear aeroelastic systems are represented by the same generalized coordinates.

3.2. State-space equations of the open-loop system

The modal-based state-space equations of the sub-linear aeroelastic systems subject to the external discrete gust excitation are commonly based on the rational function approximation of the generalized aerodynamic forces (Karpel et al., 2005). To improve the accuracy of the external discrete gust forces, a Fourier transformation of the gust profile $w_G(t)$ is implemented. Then, the inverse Fourier transformation is performed to generate a generalized gust excitation vector in time domain. For each sub-linear aeroelastic system, the differential equation corresponding to Eqs. (23)–(31) can be rewritten in the state-space form as follows:

$$\dot{\mathbf{x}}_{ae} = \mathbf{A}_{ae}\mathbf{x}_{ae} + \mathbf{B}_{ae}\mathbf{u}_{ae} + \mathbf{B}_{aw}\mathfrak{I}^{-1}\left(\left\{\mathbf{Q}_{HG}\left(\frac{i\omega L}{V}\right)\right\}\mathfrak{I}(w_G(t))\right) + \mathbf{B}_{ac}\mathbf{u}_{ac},\tag{32}$$

$$\mathbf{y}_{ae} = \mathbf{C}_{ae}\mathbf{x}_{ae} + \mathbf{D}_{ae}\mathbf{u}_{ae} + \mathbf{D}_{aw}\mathfrak{I}^{-1}\left(\left\{\mathbf{Q}_{HG}\left(\frac{i\omega L}{V}\right)\right\}\mathfrak{I}(w_G(t))\right) + \mathbf{D}_{ac}\mathbf{u}_{ac}.\tag{33}$$

The definitions of the matrices in Eqs. (32) and (33) are given in Appendix A. The basic assumption of the nonlinear aeroelastic approach in this study is that the nonlinearities in the aeroelastic system are measurable by using the two angles θ_{LEO} and θ_{TEO}, which can be computed as follows:

$$\theta_{LEO}(t) = \delta^a_{LEO}(t) - \delta^c_{LEO}(t), \quad \theta_{TEO}(t) = \delta^a_{TEO}(t) - \delta^c_{TEO}(t),\tag{34}$$

where δ_{LEO}^c and δ_{TEO}^c are the outputs of the LEO and TEO actuators, respectively. The actual deflections, δ_{LEO}^a and δ_{TEO}^a, of the LEO and TEO control surfaces can be obtained as follows:

$$\begin{Bmatrix} \delta_{\text{LEO}}^a(t) \\ \delta_{\text{TEO}}^a(t) \end{Bmatrix} = \mathbf{P}^T \mathbf{\Phi}_f \boldsymbol{\xi}_f(t).$$

4. Design of linear reduced-order controllers

In this section, two linear control systems are designed via the optimal reduced-order control scheme with unconstrained optimization techniques (Mukhopadhyay et al., 1982; Mukhopadhyay, 1990). Both of the control systems are designed based on the nominal aeroelastic system without any free-play. First, a SISO controller is designed. In this case, only the TEO control surface is used as a control actuator and the difference signal of the two accelerometers is used as the control input. Then, an MIMO controller is designed with both the LEO and TEO control surfaces as control actuators. In this case, two accelerometers are used to measure the outputs of the wind-tunnel model.

4.1. Design of a SISO controller

Fig. 5 shows the analog design that contains the basic aeroelastic model augmented with anti-aliasing filters and a first-order Pade approximation for the computational delay. If some measurement noise and a gust perturbation are assumed to be input into the aeroelastic system, then the state-space equations of the system can be written as follows:

$$\dot{\mathbf{x}} = \mathbf{A}\mathbf{x} + \mathbf{B}\mathbf{u} + \mathbf{G}_w w, \tag{35}$$

$$\mathbf{y} = \mathbf{C}\mathbf{x} + \mathsf{v}. \tag{36}$$

The cost function for controller design can be defined as

$$J = \lim_{t \to \infty} E(\mathbf{x}^T \mathbf{Q}_1 \mathbf{x} + \mathbf{u}^T \mathbf{Q}_2 \mathbf{u}), \tag{37}$$

where $\mathbf{Q}_1$ and $\mathbf{Q}_2$ are the weight coefficients to be determined. The controller is assumed to be

$$\dot{\mathbf{x}}_c = \mathbf{A}_c \mathbf{x}_c + \mathbf{B}_c \mathbf{y}, \tag{38}$$

$$\mathbf{u} = \mathbf{C}_c \mathbf{x}_c, \tag{39}$$

where $\mathbf{x}_c$ is the state of the controller of fixed orders. Now, the main task is to optimize all entries in the constant matrices $\mathbf{A}_c(s \times s)$, $\mathbf{B}_c(s \times l)$ and $\mathbf{C}_c(m \times s)$ to minimize the cost function in Eq. (37). Among all the entries in matrices $\mathbf{A}_c, \mathbf{B}_c$ and $\mathbf{C}_c$, only $s(l + m)$ of them are independent and can be chosen as design variables. The design procedure for an optimal reduced-order controller can be given as follows.

If the closed-loop system equation is represented by

$$\begin{bmatrix} \dot{\mathbf{x}}(t) \\ \dot{\mathbf{x}}_c(t) \end{bmatrix} = \begin{bmatrix} \mathbf{A} & \mathbf{B}\mathbf{C}_c \\ \mathbf{B}_c\mathbf{C} & \mathbf{A}_c \end{bmatrix} \begin{bmatrix} \mathbf{x}(t) \\ \mathbf{x}_c(t) \end{bmatrix} + \begin{bmatrix} \mathbf{G}_w & \mathbf{0} \\ \mathbf{0} & \mathbf{B}_c \end{bmatrix} \begin{Bmatrix} w \\ \mathsf{v} \end{Bmatrix}, \tag{40}$$
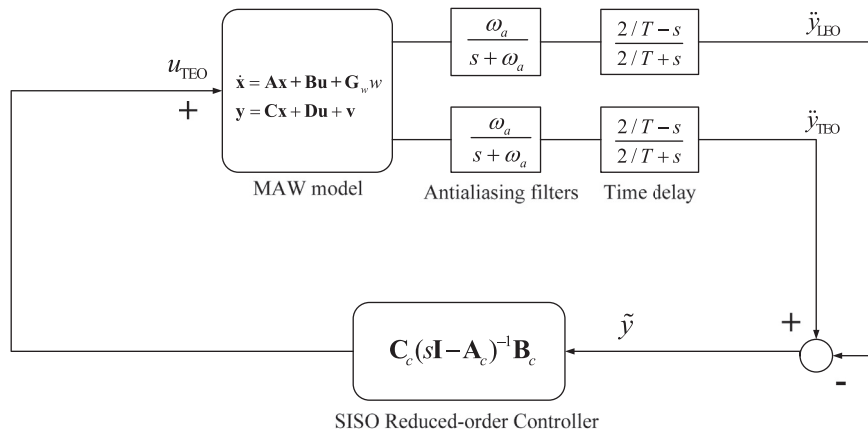

Fig. 5. Block diagram of the closed-loop aeroelastic system with a SISO reduced-order controller.

then the cost function described in Eq. (37) can be written as follows:

$$J = \lim_{t \to \infty} \mathrm{E} \left\{ \begin{bmatrix} \mathbf{x} \\ \mathbf{x}_c \end{bmatrix}^\mathrm{T} \begin{bmatrix} \mathbf{Q}_1 & \mathbf{0} \\ \mathbf{0} & \mathbf{C}_c^\mathrm{T} \mathbf{Q}_2 \mathbf{C}_c \end{bmatrix} \begin{bmatrix} \mathbf{x} \\ \mathbf{x}_c \end{bmatrix} \right\} \tag{41}$$

Utilizing Eqs. (40) and (41) and implementing the trace identity, the cost function can be recast as

$$J = \lim_{t \to \infty} \mathrm{E} \left\{ \mathrm{tr} \left\{ \begin{bmatrix} \mathbf{Q}_1 & \mathbf{0} \\ \mathbf{0} & \mathbf{C}_c^\mathrm{T} \mathbf{Q}_2 \mathbf{C}_c \end{bmatrix} \begin{bmatrix} \mathbf{x} \\ \mathbf{x}_c \end{bmatrix} \begin{bmatrix} \mathbf{x} \\ \mathbf{x}_c \end{bmatrix}^\mathrm{T} \right\} \right\} = \mathrm{tr}\{\mathbf{Q}_a \mathbf{X}_a\}, \tag{42}$$

where

$$\mathbf{Q}_a = \begin{bmatrix} \mathbf{Q}_1 & \mathbf{0} \\ \mathbf{0} & \mathbf{C}_c^\mathrm{T} \mathbf{Q}_2 \mathbf{C}_c \end{bmatrix}, \quad \mathbf{X}_a = \lim_{t \to \infty} \mathrm{E} \left\{ \mathrm{tr} \left\{ \begin{bmatrix} \mathbf{x} \\ \mathbf{x}_c \end{bmatrix} \begin{bmatrix} \mathbf{x} \\ \mathbf{x}_c \end{bmatrix}^\mathrm{T} \right\} \right\} \tag{43}$$

If the closed-loop system (40) is stable, then the covariance matrix $\mathbf{X}_a$ satisfies the Lyapunov equation given by

$$\mathbf{F}_a \mathbf{X}_a + \mathbf{X}_a \mathbf{F}_a^\mathrm{T} = -\mathbf{G}_a \mathbf{R}_a \mathbf{G}_a^\mathrm{T}, \tag{44}$$

where

$$\mathbf{F}_a = \begin{bmatrix} \mathbf{A} & \mathbf{BC}_c \\ \mathbf{B}_c \mathbf{C} & \mathbf{A}_c \end{bmatrix}, \quad \mathbf{R}_a = \begin{bmatrix} \mathbf{R}_w & \mathbf{0} \\ \mathbf{0} & \mathbf{R}_v \end{bmatrix}, \quad \mathbf{G}_a = \begin{bmatrix} \mathbf{G}_w & \mathbf{0} \\ \mathbf{0} & \mathbf{B}_c \end{bmatrix}. \tag{45}$$

There are several possible ways of selecting a set of $s(l + m)$ design variables of the control law. However, the key states must ensure that the matrix $\mathbf{F}_a$ is initially stable. In present case, the controller is designed at a flight speed of $V = 38$ m/s, and the first mode, the second mode and its derivative are selected as the three key states. The state-space equation of the resulted controller is given as follows:

$$\dot{\mathbf{x}}_c = \begin{bmatrix} -966.8 & 855.3 & -14.69 \\ 543.6 & -509.5 & 16.21 \\ -1633 & 1398 & -44.32 \end{bmatrix} \mathbf{x}_c + \begin{bmatrix} 11130 \\ 10310 \\ 0.9143 \end{bmatrix} \tilde{y}, \tag{46}$$

$$u_{\mathrm{TEO}} = \begin{bmatrix} -0.04623 & 0.03957 & -0.00093 \end{bmatrix} \mathbf{x}_c. \tag{47}$$

Fig. 6 presents the root locus of the open-loop and closed-loop aeroelastic systems with respect to the flight speeds at $V = 0, 26, 30, 34, 36, 38, 40$ and 42 m/s. The controller can expand the flutter boundary from the open-loop value of 34 m/s to 40 m/s by using only the TEO control surface as an actuator.

4.2. Design of an MIMO controller

The procedure of designing the MIMO controller is the same as that for the SISO controller. As shown in Fig. 7, two accelerometers are used in this case as the control inputs. The controller is also designed at a flight speed of $V = 38$ m/s, and the second mode, the derivative of the second mode, the fifth mode and the seventh mode are selected as the four key states
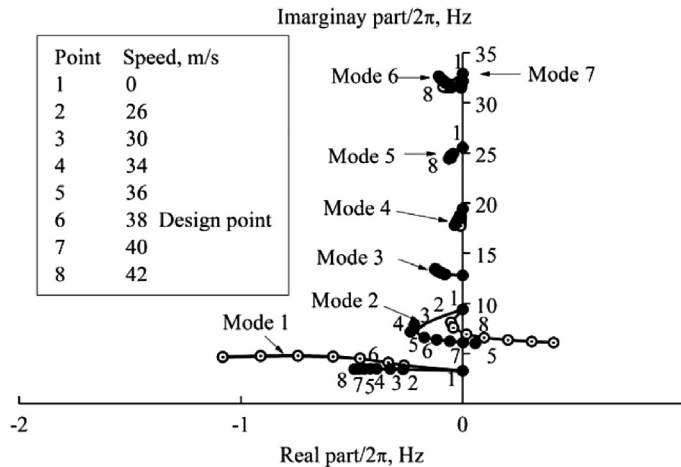

Fig. 6. The root locus of the open-loop (hollow circle) and closed-loop (solid circle) aeroelastic systems. with a speed variation at Mach 0.05 when the SISO controller is used.

Fig. 7. Block diagram of the closed-loop aeroelastic system with a MIMO reduced-order controller.

Fig. 8. The root locus of the open-loop (hollow circle) and closed-loop (solid circle) aeroelastic systems with a speed variation at Mach 0.05 when the MIMO controller is used.
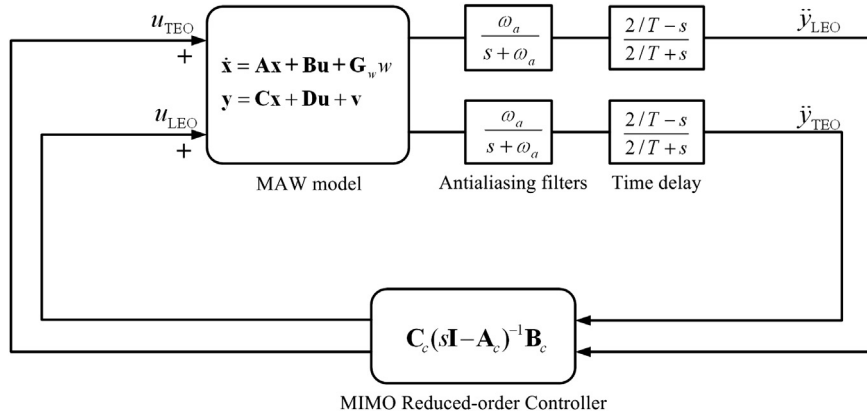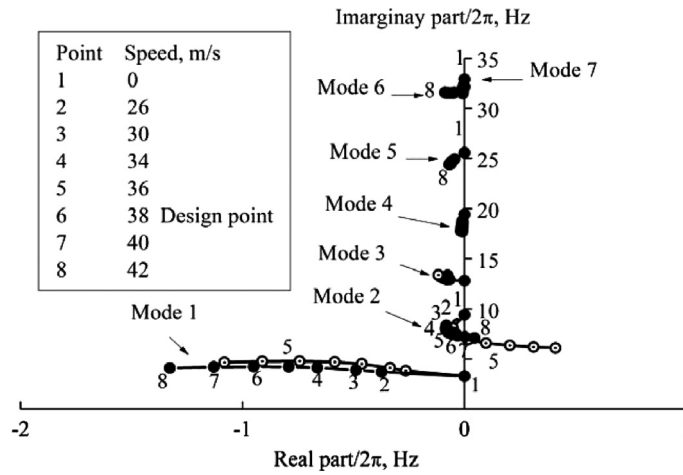
when the present control scheme is used. The MIMO controller can be expressed as

$$
\dot{\mathbf{x}}_c = \begin{bmatrix} -36.15 & -0.9364 & -0.5923 & -0.1847 \\ 484.9 & 11.09 & 3.764 & 10.79 \\ -162.1 & -3.42 & -7.92 & 46.85 \\ -497.2 & -13.77 & -39.91 & -16.59 \end{bmatrix} \mathbf{x}_c + \begin{bmatrix} -0.1109 & 0.0079 \\ -0.1408 & 0.4408 \\ -7672 & 3603 \\ 4971 & 12980 \end{bmatrix} \mathbf{y},
\tag{48}
$$

$$
\mathbf{u} = 10^{-5} \begin{bmatrix} -717.9 & -23.41 & -10.96 & -9.466 \\ -19.9 & -2.363 & -33.26 & 39.54 \end{bmatrix} \mathbf{x}_c.
\tag{49}
$$

If there is no free-play in the aeroelastic system, as shown in Fig. 8, the root loci indicate that the MIMO controller can expand the flutter boundary from the open-loop value of 34–40 m/s for the aeroelastic system without any free-play.

5. Illustrative examples

In this section, the MAW model is used as a test bed to illustrate the effects of free-plays on the open-loop and closed-loop aeroelastic systems. At first, the effects of free-plays on the open-loop aeroelastic system are studied. Then, the linear control systems, proposed in Section 4, are applied to the nonlinear aeroelastic system. As shown in Fig. 9, when solving the nonlinear aeroelastic responses, the nonlinear parameters θ_{LEO} and θ_{TEO} are first computed to find their corresponding sub-linear aeroelastic system at each time step with an interpolation scheme. For simplicity, the bilinear interpolation is used in this study. Then, the state-space equation of the corresponding sub-linear aeroelastic system is used to solve for the states in the next time step. During the simulation, the initial sates of the aeroelastic system are chosen to be zero. A discrete gust
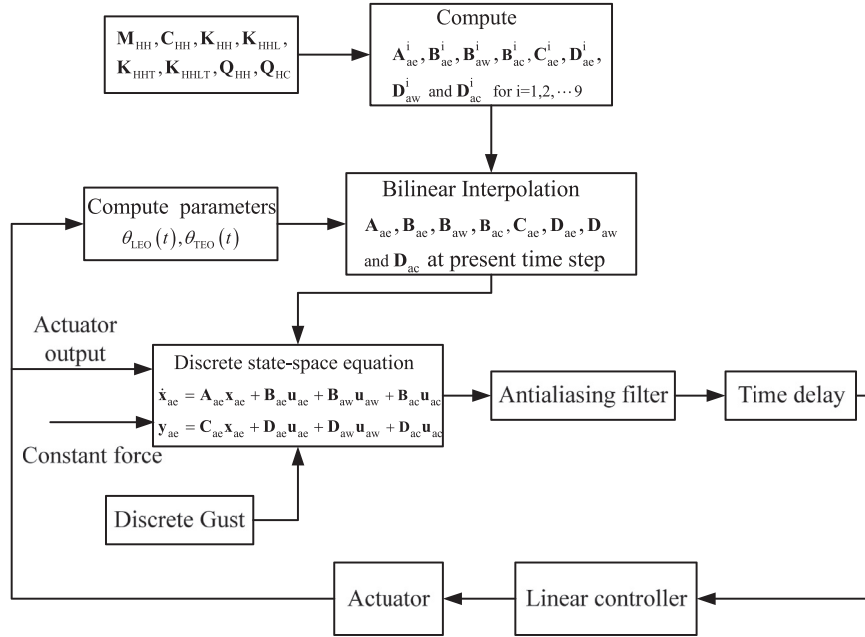
Fig. 9. Solution procedure of the transient response of the nonlinear aeroservoelastic system.
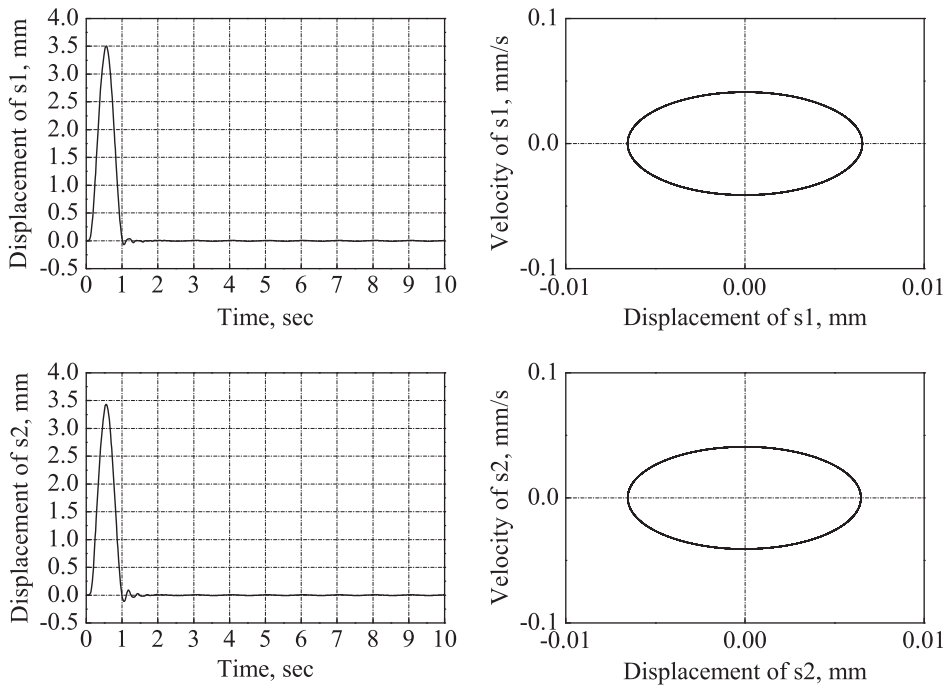
Fig. 10. Transient response and phase plot of the open-loop system with free-plays, $\delta_{LEO}=\delta_{TEO}=0.5^{\circ}$, at flight speed $V=30$ m/s.

with a one-minus-cosine profile is used as the external excitation force. The time constant of the discrete gust is chosen to be $\tau_g = 1.0$s, and the gust velocity is set to be 1% of the flight speed.

5.1. Effects of free-play on the stability of an open-loop aeroelastic system

The nonlinear aeroelastic responses of the open-loop aeroelastic system are solved for a given free-play angle, i.e., $\delta_{LEO}=\delta_{TEO}=0.5^{\circ}$. As shown in Figs. 10–13, where s1 and s2 indicate the two sensors, although the LCOs are predicted in both cases, the amplitudes of the LCOs are particularly small when the flight speed is below the flutter boundary. During the

Fig. 11. Transient response of the deflection of the LEO control surface for the open-loop system with free-plays, $\delta_{LEO}=\delta_{TEO}=0.5°$, at flight speed $V=30$ m/s.
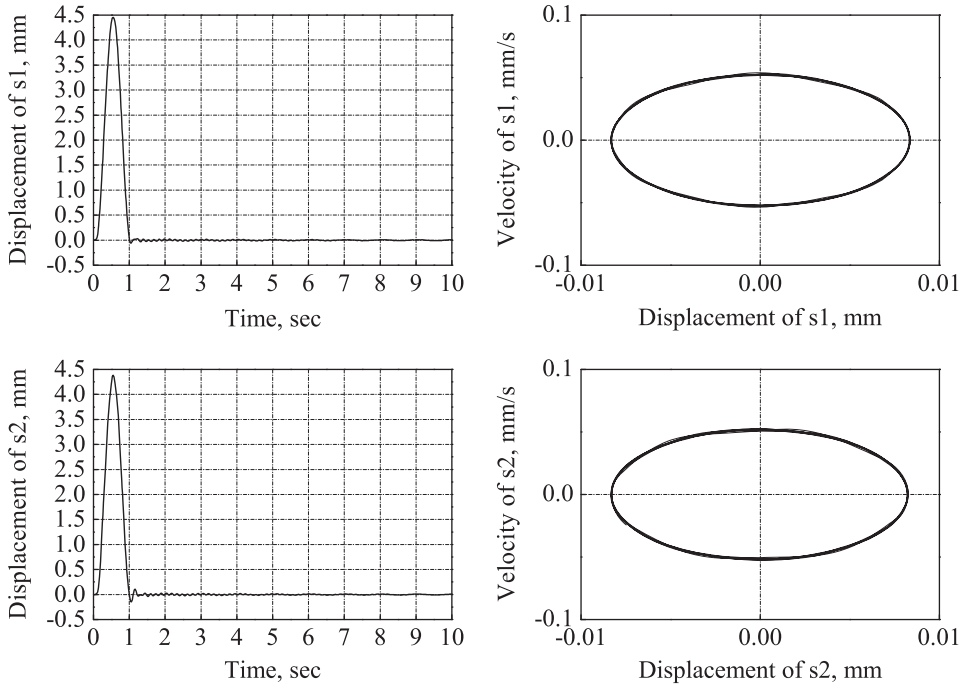
Fig. 12. Transient response and phase plot of the open-loop system with free-plays, $\delta_{LEO}=\delta_{TEO}=0.5°$, at flight speed $V=34$ m/s.

simulation, when the flight speed slightly exceeds 34 m/s, the open-loop system becomes unstable. Thus, the numerical simulations in this sub-section illustrate that a variety of LCOs can be observed when the free-plays appear in both LEO and TEO control surfaces of a three-dimensional aeroelastic system. To investigate the nonlinear aeroelastic characteristics of the MAW model with multiple free-plays, the time responses of the nonlinear aeroelastic system are solved with an increase of the flight speed. Fig. 14 shows the LCO amplitudes of the MAW model with multiple free-play nonlinearities observed in the nonlinear aeroelastic analysis. As shown in Fig. 14, the LCO amplitude of the MAW model is getting larger and larger as an increase of the flight speed. However, the linear flutter phenomenon is observed when the flight speed exceeds the linear flutter boundary.
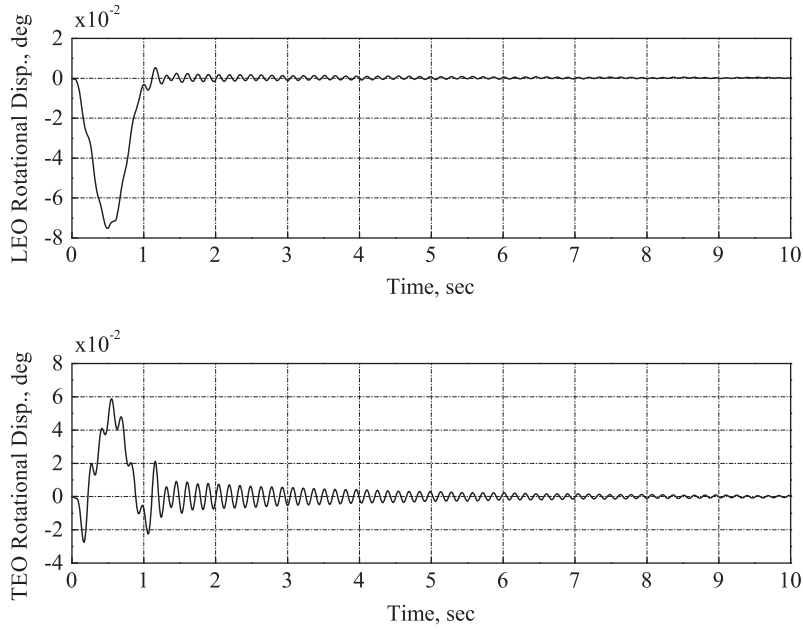
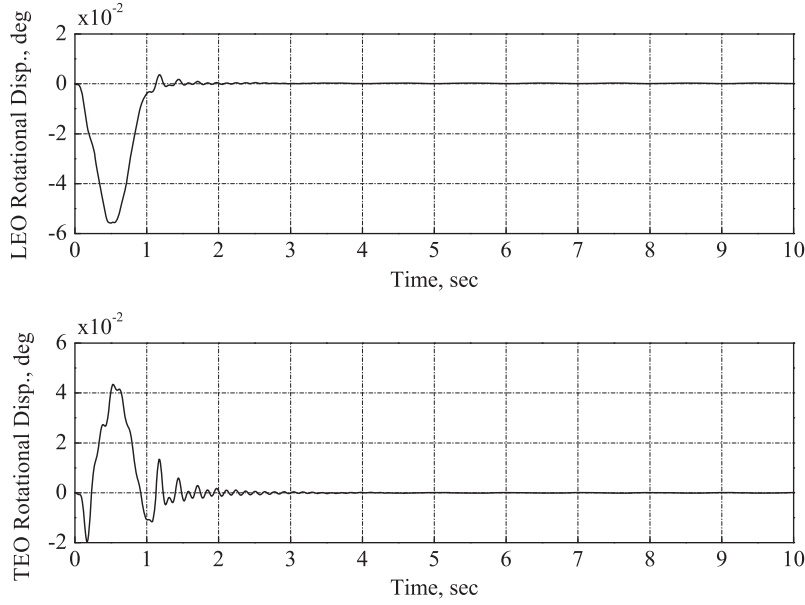**Fig. 13.** Transient response of the deflection of the LEO control surface for free-plays $\delta_{LEO}=\delta_{TEO}=0.5°$, at flight speed $V=34$ m/s.
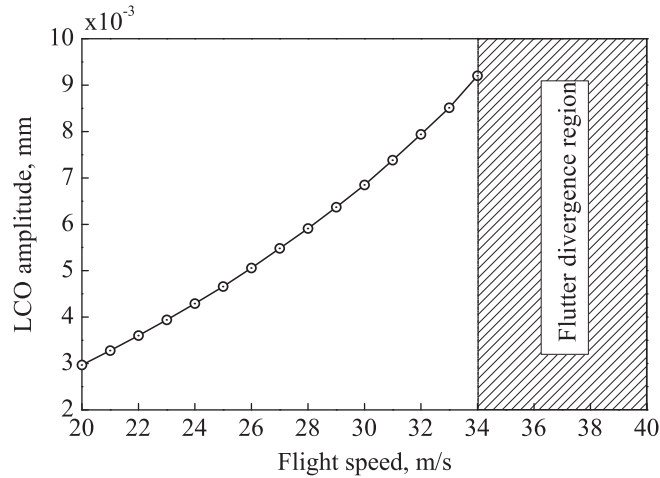
Fig. 14. LCO amplitudes of the MAW model with multiple free-play nonlinearities.

5.2. Effects of free-play on the stability of a closed-loop aeroelastic system

This sub-section focuses on the effects of the free-play nonlinearities on the proposed linear control systems in two case studies, where a linear SISO controller and a linear MIMO controller are implemented, respectively. In these two cases, the free-plays in both LEO and TEO control surfaces are considered.

In the first case study, the SISO control law is implemented on the nonlinear aeroelastic system, where only the TEO control surface is actuated to suppress the flutter of the system, and the difference between sensor 1 and sensor 2 is used as a feedback signal. The SISO controller is implemented on the nonlinear aeroelastic system with the fixed free-play angles, i. e., $\delta_{LEO}=\delta_{TEO}=0.5°$. The system is kept in an open loop case for $t=2.0$s, and then the loop is closed. At $t=2.0$s, the actuator is switched on to actuate the TEO control surface. Figs. 15–17 show the transient responses of the closed-loop system at $V=34$, 35 and 36 m/s, respectively when the SISO controller is used. As shown in these figures, the instability of the aeroelastic system can be suppressed although the system contains free-plays in both LEO and TEO control surfaces. As these figures show, however, that the time responses of sensor 1 and sensor 2 cannot converge to zero. This phenomenon can be explained as follows. The hinge moment of the actuator equals to zero when the control surface passes through to the free-play zone. Thus, the time responses of the closed-loop system are divergent until the control surface is kept away from the free-play zone. In this case, the closed-loop system may be unstable until the nonlinear parameter of the TEO control
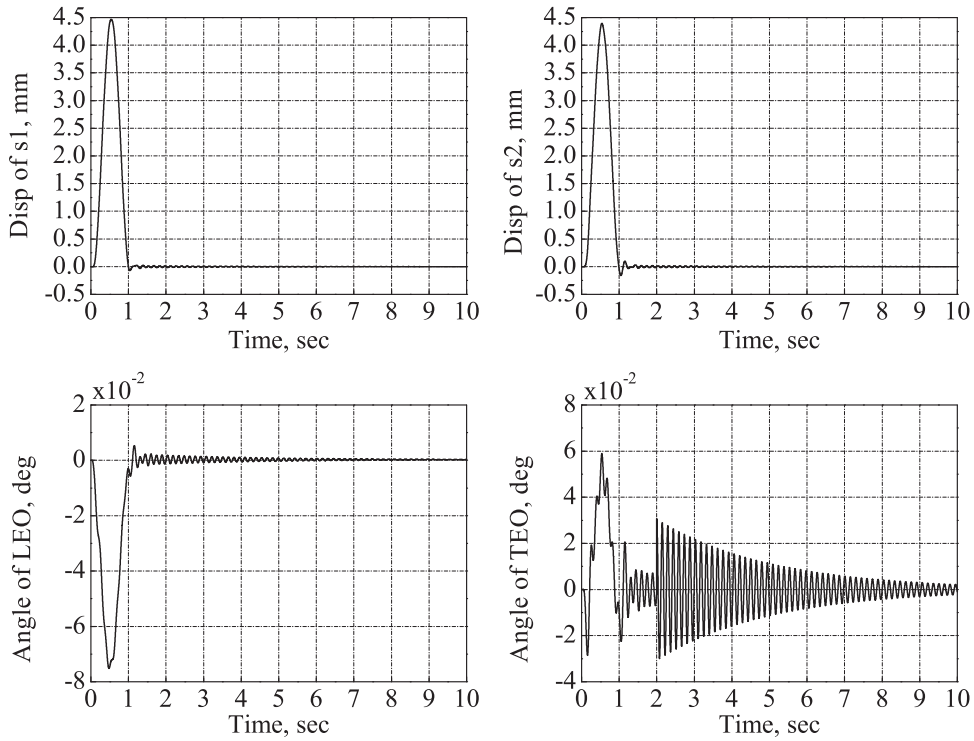
Fig. 15. Transient responses of the closed-loop system with free-plays, $\delta_{LEO}=\delta_{TEO}=0.5°$, at flight speed $V=34$ m/s when the SISO controller is used.

**Fig. 16.** Transient responses of the closed-loop system with free-plays, $\delta_{LEO}=\delta_{TEO}=0.5°$, at flight speed $V=35$ m/s when the SISO controller is used.

surface is outside the free-play zone. Fig. 18 shows the time responses of the closed-loop system with free-plays at a flight speed of $V=38$ m/s. The figure illustrates that the closed-loop system is unstable when the SISO controller is implemented. Compared with the linear results shown in Fig. 6, one finds that the free-plays in both LEO and TEO control surfaces decrease

Fig. 17. Transient responses of the closed-loop system with free-plays, $\delta_{LEO} = \delta_{TEO} = 0.5°$, at flight speed $V = 36$ m/s when the SISO controller is used.
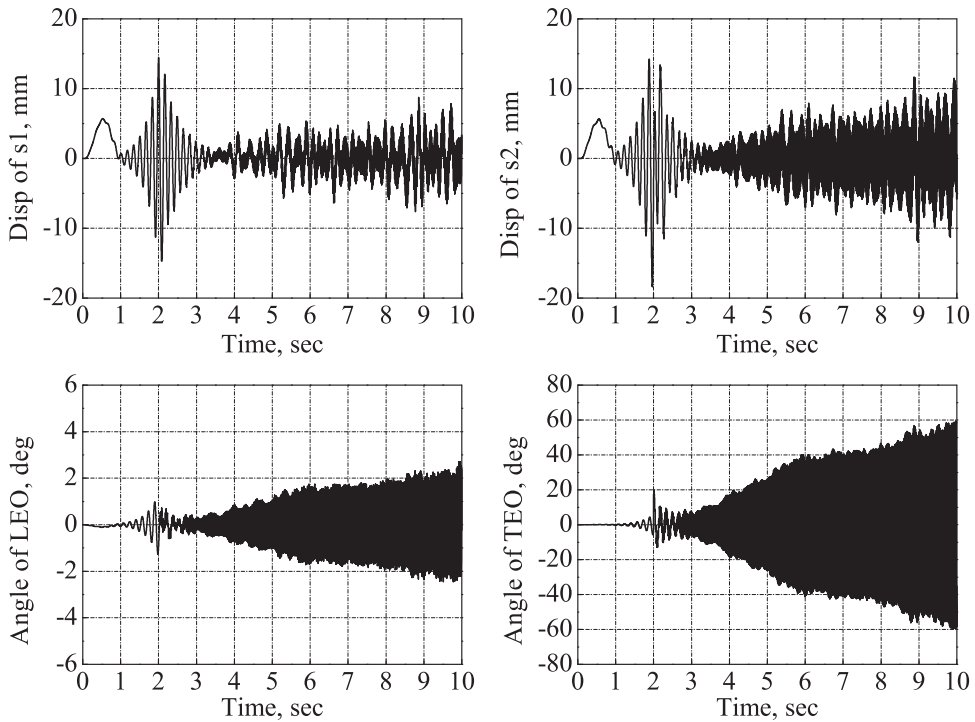
Fig. 18. Transient responses of the closed-loop system with free-plays, $\delta_{LEO} = \delta_{TEO} = 0.5°$, at flight speed $V = 38$ m/s when the SISO controller is used.

the flutter boundary of the closed-loop system. Fig. 19 presents the FFT spectrums of the outputs of sensors and the rotation of control surfaces for $V = 38$ m/s. The figure shows that the input and output signals of the closed-loop system contain a high frequency component when the flight speed is higher than 38 m/s. This case demonstrates that the linear SISO
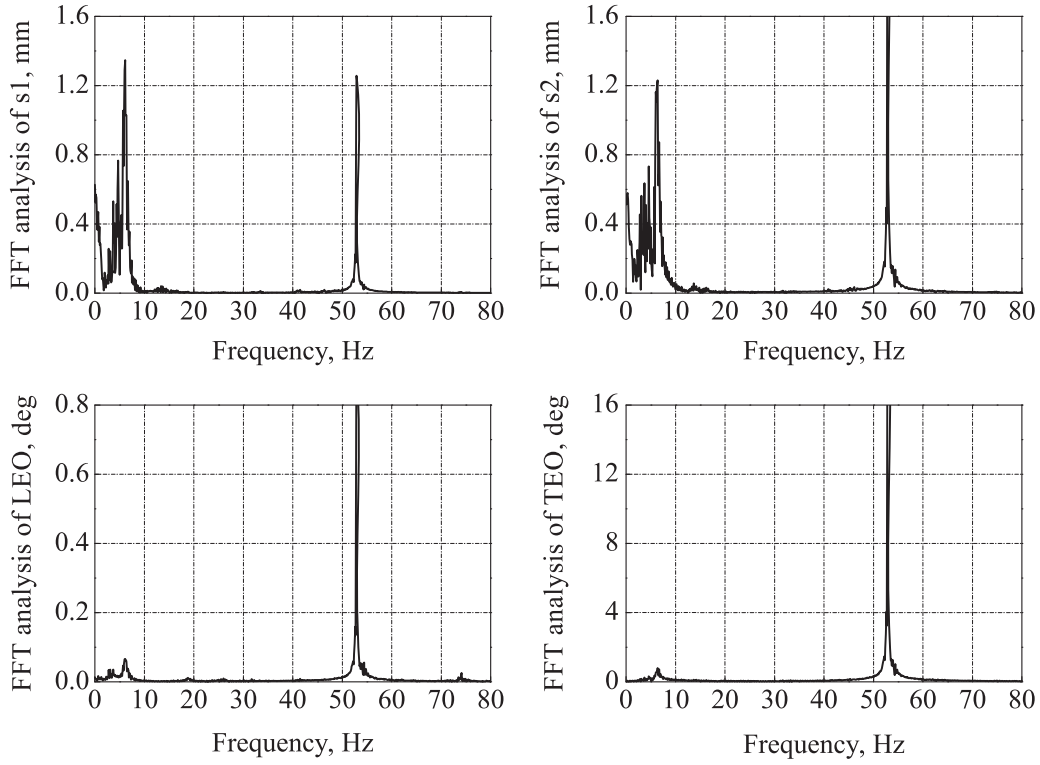
Fig. 19. FFT spectrums of the transient responses of the closed-loop system with free-plays, $\delta_{LEO}=\delta_{TEO}=0.5°$, at flight speed $V=38$ m/s when the SISO controller is used.
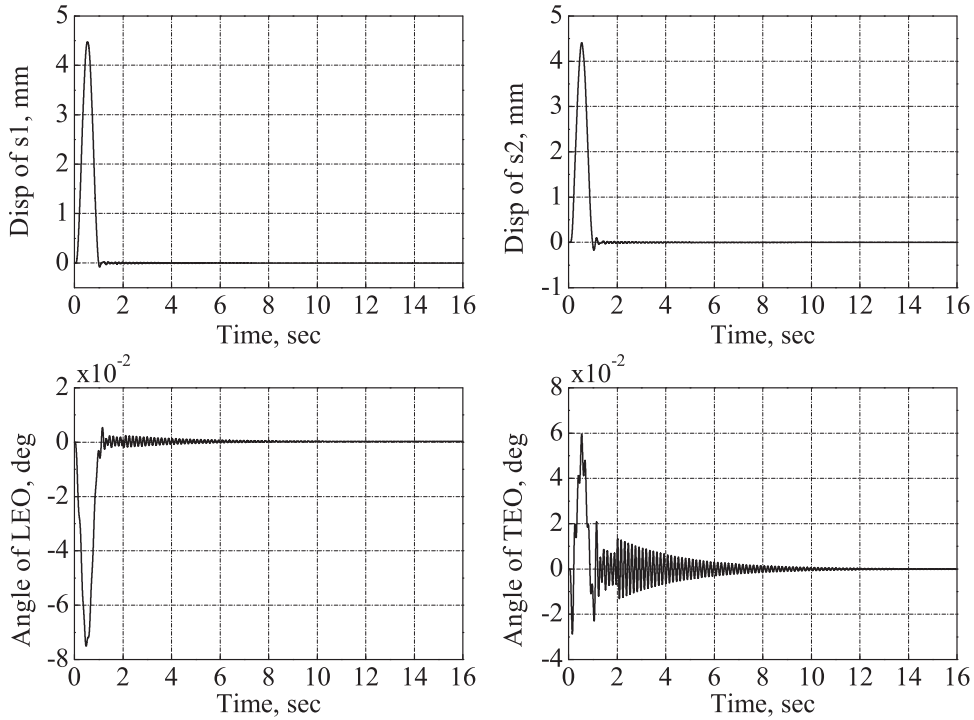
Fig. 20. Transient responses of the closed-loop system with free-plays, $\delta_{LEO}=\delta_{TEO}=0.5°$, at flight speed $V=34$ m/s when the MIMO controller is used.
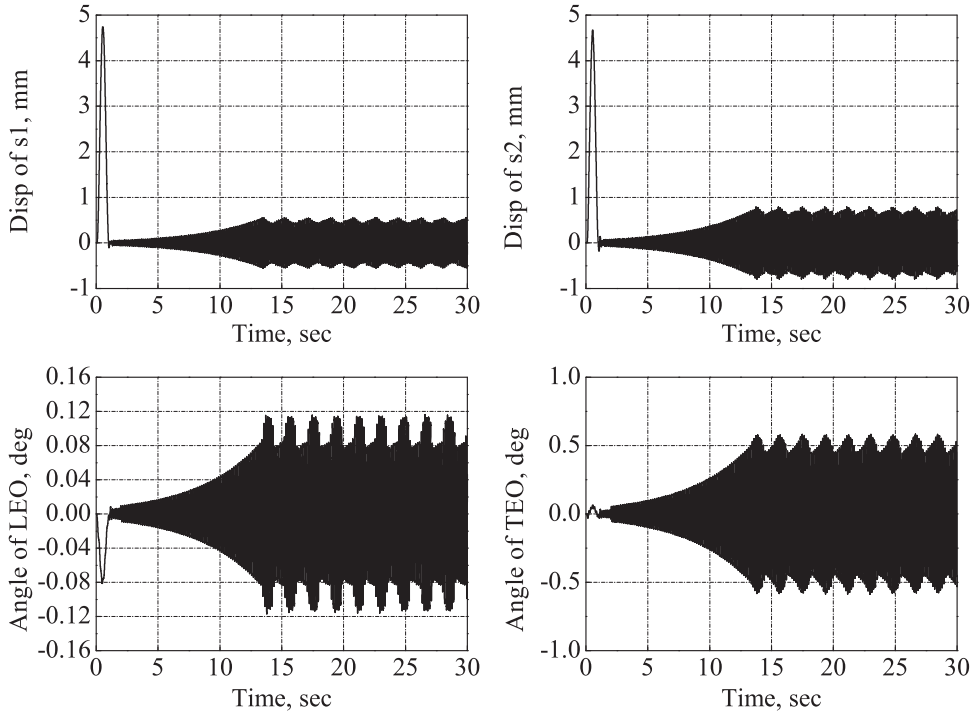
Fig. 21. Transient responses of the closed-loop system with free-plays, $\delta_{LEO}=\delta_{TEO}=0.5°$, at flight speed $V=35$ m/s when the MIMO controller is used.
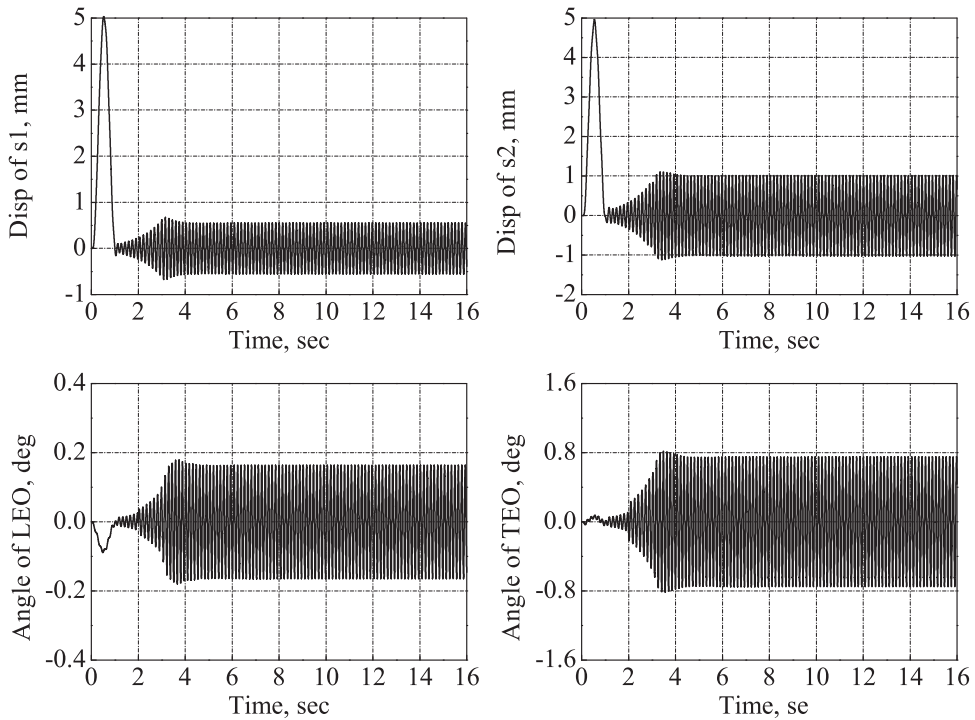
Fig. 22. Transient responses of the closed-loop system with free-plays, $\delta_{LEO}=\delta_{TEO}=0.5°$, at flight speed $V=36$ m/s when the MIMO controller is used.

controller can still be used to suppress the flutter instability of the three-dimensional aeroelastic system with free-plays in both LEO and TEO control surfaces, but the flutter boundary of the closed-loop system decreases due to the effect of free-plays.

The second case study is performed with the MIMO controller. As shown in Fig. 7, the accelerations measured by sensors 1 and 2 are used as feedback signals, and both LEO and TEO control surfaces are actuated as control inputs to suppress the flutter instability of the system. As in the first case, the system is kept in an open loop status before $t = 2.0$s, and then the loop is closed. At $t = 2.0$s, the actuators are switched on to actuate both LEO and TEO control surfaces. Fig. 20 presents the
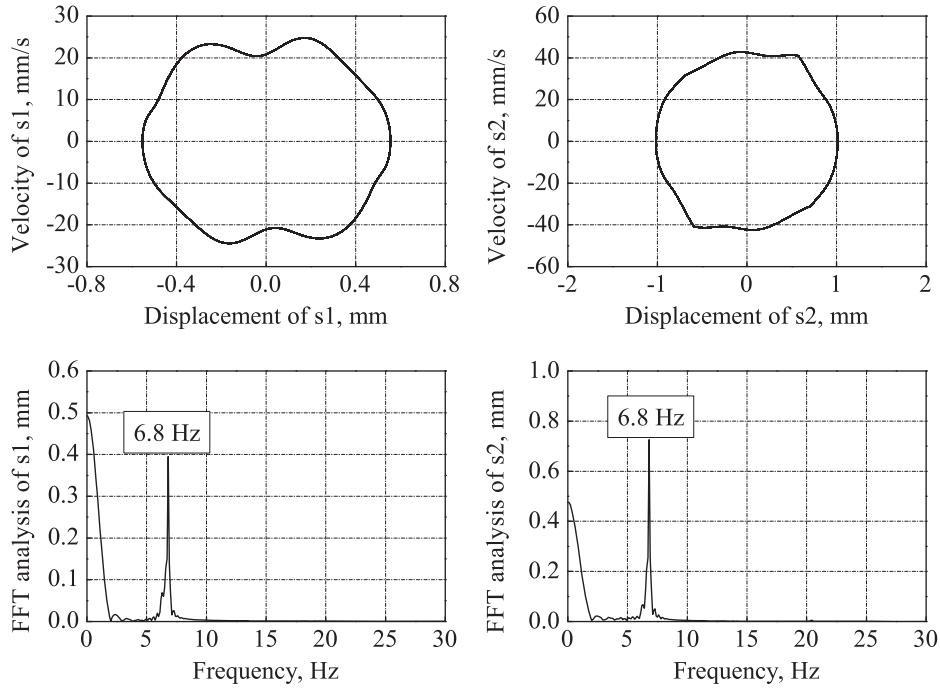
**Fig. 23.** Phase plots and FFT spectrums of the sensor outputs at flight speed V=36 m/s.
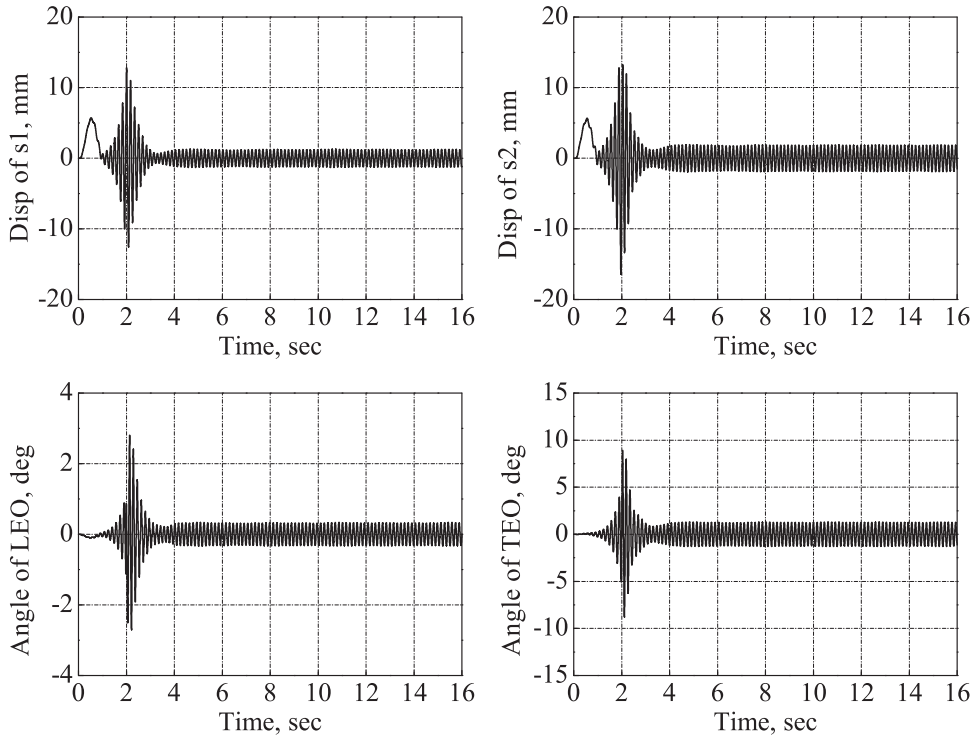
Fig. 24. Transient responses of the closed-loop system with free-plays, $\delta_{LEO} = \delta_{TEO} = 0.5°$, at flight speed $V = 38$ m/s when the MIMO controller is used.
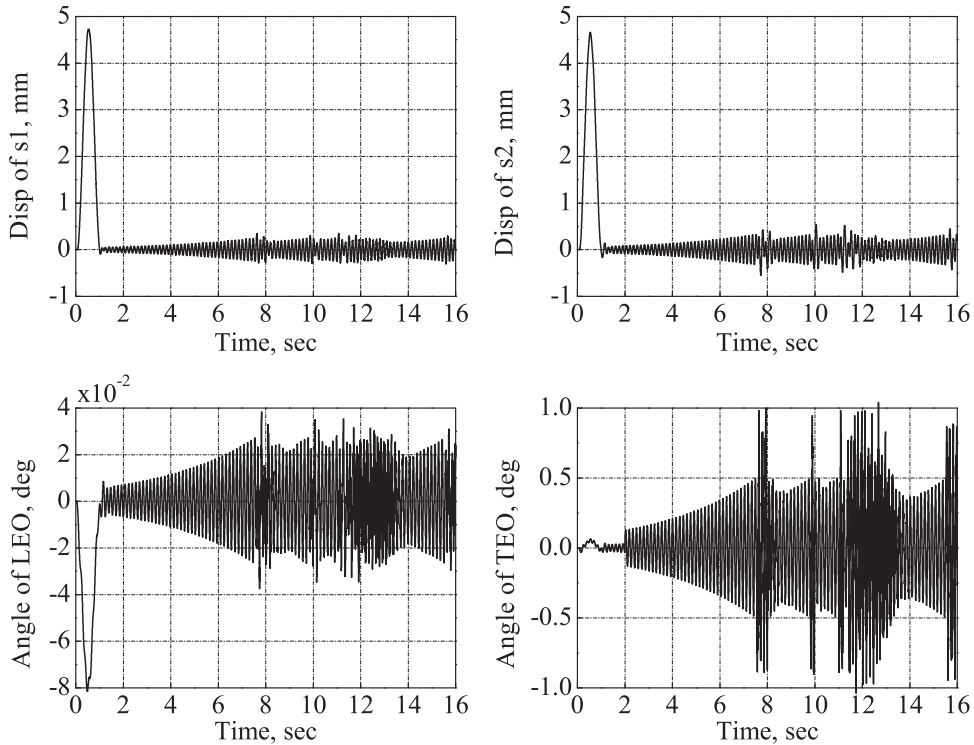
time responses of the closed-loop system at the pre-flutter speed of $V=34$ m/s. Because the nonlinear parameters θ_{LEO} and θ_{TEO} are within the free-play zone, the hinge moments of the LEO and TEO actuators equal to zero. Thus, the time responses of the closed-loop system are the same as those of open-loop system as shown in Fig. 12. Fig. 21 shows that the instability of the aeroelastic system with free-plays in both LEO and TEO control surfaces can also be suppressed at $V=35$ m/s via the
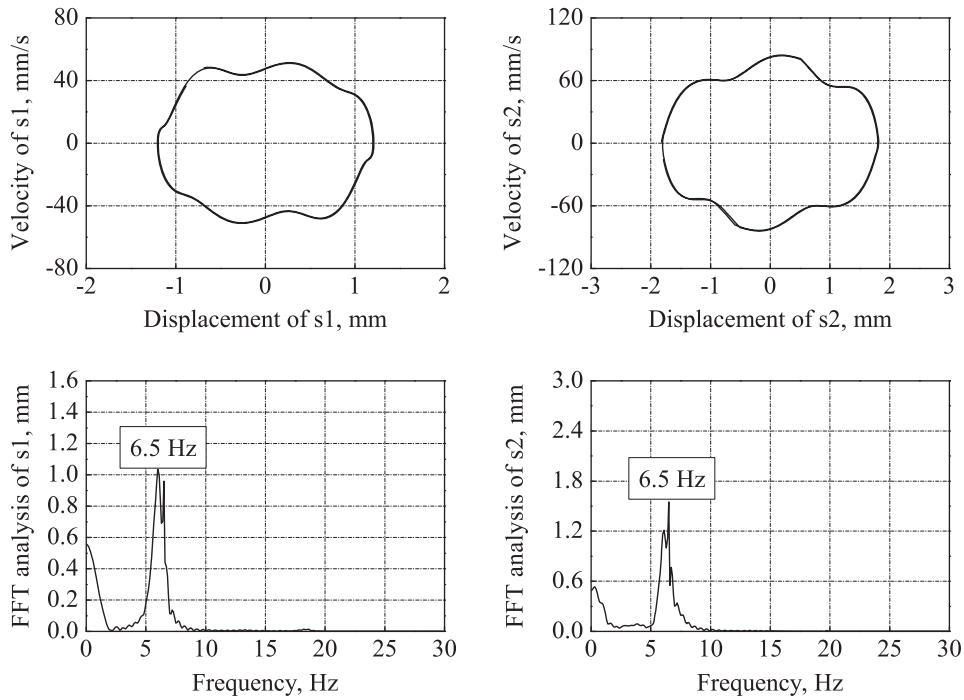
Fig. 25. Phase plots and FFT spectrums of sensor outputs at flight speed $V=38$ m/s.
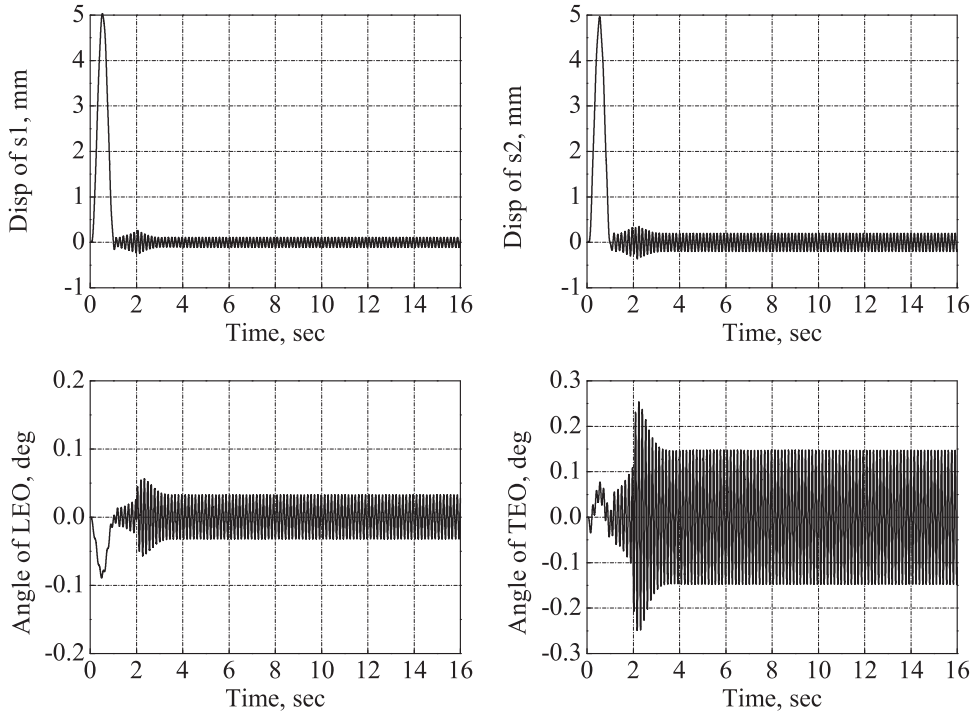
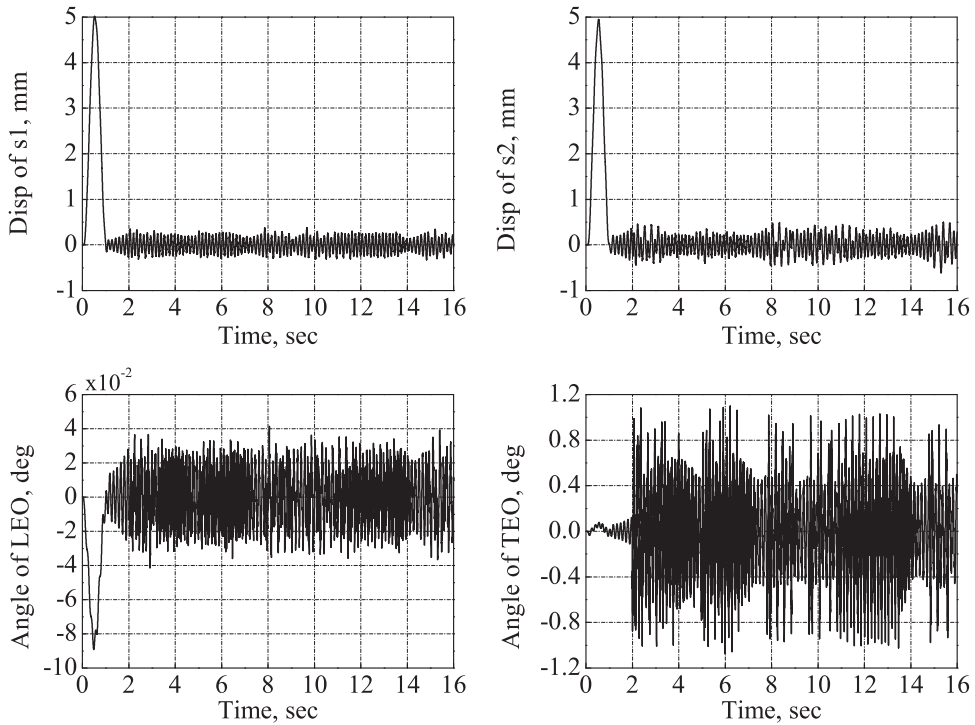**Fig. 26.** Transient responses of the closed-loop system with free-plays, $\delta_{LEO}=\delta_{TEO}=0.1°$, at flight speed $V=36$ m/s when the MIMO controller is used.
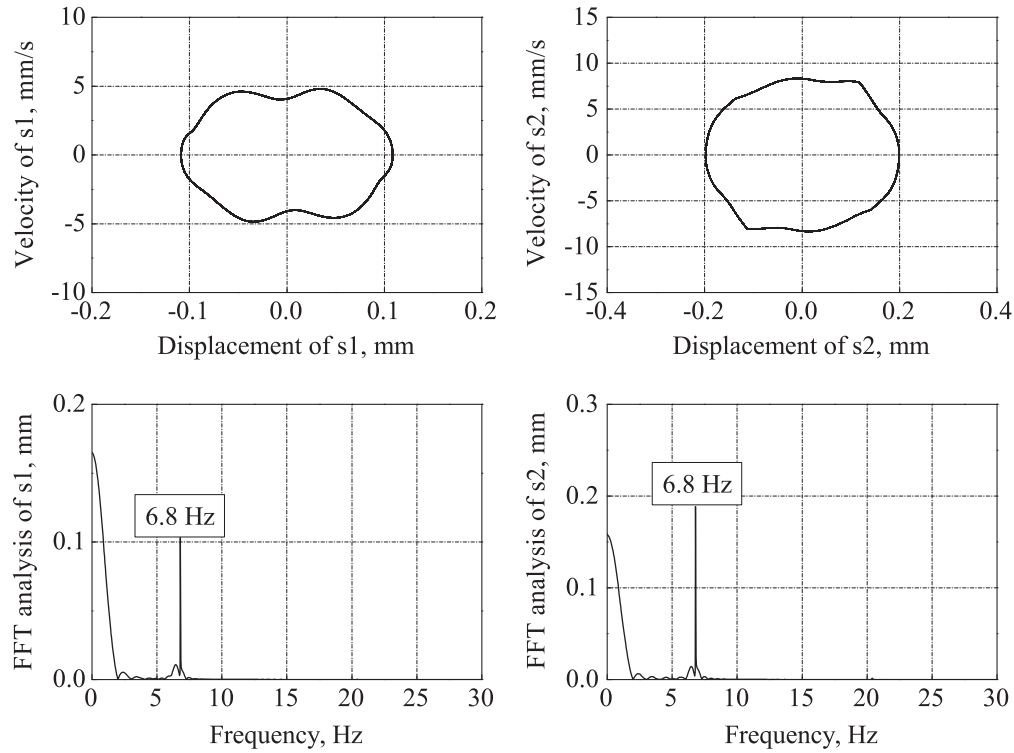
Fig. 27. Phase plots and FFT spectrums of the sensor outputs for $\delta_{LEO}=\delta_{TEO}=0.1°$, $V=36$ m/s, when the MIMO controller is used.

linear MIMO controller. As in the first case, however, the time responses cannot converge to zero. The explanation of this phenomenon is the same as the first case. Figs. 22 and 24 present the time responses of the closed-loop system with free-plays $\delta_{LEO}=\delta_{TEO}=0.5°$ at $V=36$ and 38 m/s, respectively when the MIMO controller is used. The instability of the closed-loop system is suppressed at these two speeds, but the LCO is observed at these two flight speeds. Figs. 23 and 25 show the phase plots and FFT spectrums of the outputs of sensors at flight speeds of $V=36$ and 38 m/s, respectively. These two figures indicate that the amplitude of the LCO increases with the flight speed, while the frequency of the LCO decreases slightly from 6.8 Hz to 6.5 Hz. This case illustrates that the linear MIMO controller can still be used to suppress the flutter instability of the aeroelastic system with free-plays in both LEO and TEO actuators. In contrast to the linear results, however, two points can be predicted. First, relative to the linear flutter boundary without any free-play, the flutter boundary of a closed-loop system with free-plays may be decreased. Then, the LCO is observed when the MIMO controller is implemented on the three-dimensional aeroelastic system with free-plays. As the flight speed increases, the amplitude and frequency of the LCO increases and decreases, respectively. It should be noted that the aerodynamic nonlinearities, caused by the free-play of $0.5°$ in the LEO and TEO control surfaces, are not taken into consideration during the simulation. However, the present results still provide useful information for the nonlinear aeroservoelastic analysis of the three-dimensional aeroelastic system with free-plays. For comparison, the MIMO controller is implemented for the nonlinear aeroelastic system with a much less free-play angle of $0.1°$ in the LEO and TEO control surfaces. Similar to Figs. 22 and 23, Figs. 26 and 27 show the time responses and phase plots of the closed-loop aeroelastic system for $\delta_{LEO}=\delta_{TEO}=0.1°$, $V=36$ m/s, respectively. These two figures demonstrate that the LCO is still observed even the aeroelastic system contains two small free-play angles, say, $0.1°$ in the LEO and TEO control surfaces. Compared with those for $\delta_{LEO}=\delta_{TEO}=0.5°$, the LCO magnitude decreases as the free-plays decreases.

6. Conclusions

This paper presents the study on the effects of free-play nonlinearities on the linear flutter control system of a three-dimensional aeroelastic system, where both LEO and TEO control surfaces have a free-play in their flaps. With the help of the fictitious mass approach, the nonlinear aeroelastic system can be described as a piecewise linear aeroelastic system. Based on the sub-linear aeroelastic systems, the nonlinear aeroelastic responses of the open/closed-loop aeroelastic system with free-plays can be solved. To demonstrate the effects of the free-play nonlinearities on the linear control system of the three-dimensional aeroelastic system, two reduced-order optimal controllers, i.e., a Single-Input and Single-Output (SISO) controller and a Multi-Input and Multi-Output (MIMO) controller, are designed via the unconstrained optimization

techniques. Numerical results show that when only the TEO control surface is actuated as a control input for the SISO controller, the linear control system can still work. However, the flutter velocity of the closed-loop system with free-plays is lower than that of the corresponding system without any free-play. Similar to the SISO controller, when the MIMO controller is implemented on the high-dimensional aeroelastic system with free-plays in both LEO and TEO actuators, the control system is still effective, but the flutter boundary becomes lower. Moreover, the LCOs are predictable at the linear post-flutter velocities when the MIMO controller is used.

Acknowledgments

Appendix A

Utilizing a rational function approximation, the generalized aerodynamic matrices can be approximated as follows:

$$[\mathbf{Q}_{HH} \quad \mathbf{Q}_{HC}] = \mathbf{A}_0 + \frac{b}{V}\mathbf{A}_1 s + \frac{b^2}{V^2}\mathbf{A}_2 s^2 + \mathbf{D}\left(\mathbf{I}s - \frac{V}{b}\mathbf{R}\right)^{-1}\mathbf{E}s, \tag{A.1}$$

where

$$\mathbf{E} = [\mathbf{E}_s \quad \mathbf{E}_c], \quad \mathbf{A}_i = [\mathbf{A}_{s_i} \quad \mathbf{A}_{c_i}], \quad i = 0, 1, 2. \tag{A.2}$$

The dynamic equation in Eq. (23) can be rewritten as

$$\left(\mathbf{M}_{HH} - q_d \frac{b^2}{V^2}\mathbf{A}_{s_2}\right)\ddot{\boldsymbol{\xi}}_f + \left(\mathbf{C}_{HH} - q_d \frac{b}{V}\mathbf{A}_{s_1}\right)\dot{\boldsymbol{\xi}}_f + (\mathbf{K}_{HH} - q_d \mathbf{A}_{s_0})\boldsymbol{\xi}_f - q_d \mathbf{D}\mathbf{X}_a$$

$$+ \left(\mathbf{M}_{HC} - q_d \frac{b^2}{V^2}\mathbf{A}_{c_2}\right)\ddot{\boldsymbol{\delta}} - q_d \frac{b}{V}\mathbf{A}_{c_1}\dot{\boldsymbol{\delta}} - q_d \mathbf{A}_{c_0}\boldsymbol{\delta} = \mathbf{F}_g + \boldsymbol{\Phi}_f^T[\mathbf{K}_{NM} - \mathbf{K}_{LT}]\{\delta_{1p2}\}. \tag{A.3}$$

Eq. (A.3) can be used to derive the linear aeroelastic equations in the state space into the following set of linearized differential equations

$$\begin{cases} \dot{\mathbf{x}}_{ae} = \mathbf{A}_{ae}\mathbf{x}_{ae} + \mathbf{B}_{ae}\mathbf{u}_{ae} + \mathbf{B}_{aw}\mathfrak{I}^{-1}\left(\left\{\mathbf{Q}_{HG}\left(\frac{i\omega L}{V}\right)\right\}\mathfrak{I}(w_G(t))\right) + \mathbf{B}_{ac}\{\delta_{1p2}\}, \\ \mathbf{y}_{ae} = \mathbf{C}_{ae}\mathbf{x}_{ae} + \mathbf{D}_{ae}\mathbf{u}_{ae} + \mathbf{D}_{aw}\mathfrak{I}^{-1}\left(\left\{\mathbf{Q}_{HG}\left(\frac{i\omega L}{V}\right)\right\}\mathfrak{I}(w_G(t))\right) + \mathbf{D}_{ac}\{\delta_{1p2}\} \end{cases}, \tag{A.4}$$

where the aerodynamic state vector $\mathbf{X}_a$ is defined as

$$\dot{\mathbf{X}}_a = \frac{V}{b}\mathbf{R}\mathbf{X}_a + \mathbf{E}_s\{\dot{\boldsymbol{\xi}}\} + \mathbf{E}_c\{\dot{\boldsymbol{\delta}}\}. \tag{A.5}$$

The matrices of the linearized differential equations are given as

$$\mathbf{A}_{ae} = \begin{bmatrix} \mathbf{0} & \mathbf{I} & \mathbf{0} \\ -\overline{\mathbf{M}}_{HH}^{-1}(\mathbf{K}_{HH} + q_d\mathbf{A}_{s_0}) & -\overline{\mathbf{M}}_{HH}^{-1}\left(\mathbf{C}_{HH} + q_d\frac{b}{V}\mathbf{A}_{s_1}\right) & -q_d\overline{\mathbf{M}}_{HH}^{-1}\mathbf{D} \\ \mathbf{0} & \mathbf{E}_s & \frac{V}{b}\mathbf{R} \end{bmatrix}, \mathbf{B}_{ac} = \begin{bmatrix} \mathbf{0} \\ \overline{\mathbf{M}}_{HH}^{-1}\boldsymbol{\Phi}_f^T \\ \mathbf{0} \end{bmatrix}[\mathbf{K}_{NM} - \mathbf{K}_{LT}], , \tag{A.6}$$

$$\mathbf{B}_{ae} = \begin{bmatrix} \mathbf{0} & \mathbf{0} & \mathbf{0} \\ -q_d\overline{\mathbf{M}}_{HH}^{-1}\mathbf{A}_{c_0} & -q_d\frac{b}{V}\overline{\mathbf{M}}_{HH}^{-1}\mathbf{A}_{c_1} & -\overline{\mathbf{M}}_{HH}^{-1}\left(\mathbf{M}_{HC} + q_d\frac{b^2}{V^2}\mathbf{A}_{c_2}\right) \\ \mathbf{0} & \mathbf{E}_c & \mathbf{0} \end{bmatrix}, \mathbf{B}_{aw} = \begin{bmatrix} \mathbf{0} \\ -\frac{q_d}{V}\overline{\mathbf{M}}_{HH}^{-1} \\ \mathbf{0} \end{bmatrix}, \tag{A.7}$$

$$\mathbf{x}_{ae} = \begin{Bmatrix} \boldsymbol{\xi}_f \\ \dot{\boldsymbol{\xi}}_f \\ \mathbf{X}_a \end{Bmatrix}, \mathbf{u}_{ae} = \begin{Bmatrix} \boldsymbol{\delta} \\ \dot{\boldsymbol{\delta}} \\ \ddot{\boldsymbol{\delta}} \end{Bmatrix}, \boldsymbol{\delta} = \begin{Bmatrix} \delta_{LEO}^c \\ \delta_{TEO}^c \end{Bmatrix}, \overline{\mathbf{M}}_{HH} = \mathbf{M}_{HH} + q_d\frac{b^2}{V^2}\mathbf{A}_{s_2}. \tag{A.8}$$

The matrices $\mathbf{C}_{ae}, \mathbf{D}_{ae}$ $\mathbf{D}_{aw}$ and $\mathbf{D}_{ac}$ in Eq. (A.4) are as following

$$\mathbf{C}_{ae} = \boldsymbol{\Phi}_s\left[-\overline{\mathbf{M}}_{HH}^{-1}(\mathbf{K}_{HH} + q_d\mathbf{A}_{s_0}) \quad -\overline{\mathbf{M}}_{HH}^{-1}\left(\mathbf{C}_{HH} + q_d\frac{b}{V}\mathbf{A}_{s_1}\right) \quad -q_d\overline{\mathbf{M}}_{HH}^{-1}\mathbf{D}\right], \mathbf{D}_{ac} = \boldsymbol{\Phi}_s\overline{\mathbf{M}}_{HH}^{-1}\boldsymbol{\Phi}_f^T[\mathbf{K}_{NM} - \mathbf{K}_{LT}], \tag{A.9}$$

$$\mathbf{D}_{ae} = \boldsymbol{\Phi}_s\left[-q_d\overline{\mathbf{M}}_{HH}^{-1}\mathbf{A}_{c_0} \quad -q_d\frac{b}{V}\overline{\mathbf{M}}_{HH}^{-1}\mathbf{A}_{c_1} \quad -\overline{\mathbf{M}}_{HH}^{-1}\left(\mathbf{M}_{HC} + q_d\frac{b^2}{V^2}\mathbf{A}_{c_2}\right)\right], \mathbf{D}_{aw} = \boldsymbol{\Phi}_s\left[-\frac{q_d}{V}\overline{\mathbf{M}}_{HH}^{-1}\right], \tag{A.10}$$

where $\boldsymbol{\Phi}_s$ is the modal displacement matrix at the sensor location.

Given free-plays, Eq. (A.4) falls into one of the following nine cases:

(1) For $\theta_{LEO} > \delta_{LEO}$ and $\theta_{TEO} > \delta_{TEO}$:

$$\begin{cases} \dot{\mathbf{x}}_{ae} = \mathbf{A}_{ae}\mathbf{x}_{ae} + \mathbf{B}_{ae}\mathbf{u}_{ae} + \mathbf{B}_{aw}\mathfrak{I}^{-1}\left(\left\{\mathbf{Q}_{HG}\left(\frac{i\omega L}{V}\right)\right\}\mathfrak{I}(w_G(t))\right) + \mathbf{B}_{ac}\{\delta_{1p2}\}, \\ \mathbf{y}_{ae} = \mathbf{C}_{ae}\mathbf{x}_{ae} + \mathbf{D}_{ae}\mathbf{u}_{ae} + \mathbf{D}_{aw}\mathfrak{I}^{-1}\left(\left\{\mathbf{Q}_{HG}\left(\frac{i\omega L}{V}\right)\right\}\mathfrak{I}(w_G(t))\right) + \mathbf{D}_{ac}\{\delta_{1p2}\} \end{cases}. \qquad (A.11)$$

(2) For $\theta_{LEO} < -\delta_{LEO}$ and $\theta_{TEO} < -\delta_{TEO}$:

$$\begin{cases} \dot{\mathbf{x}}_{ae} = \mathbf{A}_{ae}\mathbf{x}_{ae} + \mathbf{B}_{ae}\mathbf{u}_{ae} + \mathbf{B}_{aw}\mathfrak{I}^{-1}\left(\left\{\mathbf{Q}_{HG}\left(\frac{i\omega L}{V}\right)\right\}\mathfrak{I}(w_G(t))\right) + \mathbf{B}_{ac}\{-\delta_{1p2}\}, \\ \dot{\mathbf{x}}_{ae} = \mathbf{A}_{ae}\mathbf{x}_{ae} + \mathbf{B}_{ae}\mathbf{u}_{ae} + \mathbf{B}_{aw}\mathfrak{I}^{-1}\left(\left\{\mathbf{Q}_{HG}\left(\frac{i\omega L}{V}\right)\right\}\mathfrak{I}(w_G(t))\right) + \mathbf{B}_{ac}\{-\delta_{1p2}\}, \end{cases} \qquad (A.12)$$

(3) For $\theta_{LEO} > \delta_{LEO}$ and $\theta_{TEO} < -\delta_{TEO}$:

$$\begin{cases} \dot{\mathbf{x}}_{ae} = \mathbf{A}_{ae}\mathbf{x}_{ae} + \mathbf{B}_{ae}\mathbf{u}_{ae} + \mathbf{B}_{aw}\mathfrak{I}^{-1}\left(\left\{\mathbf{Q}_{HG}\left(\frac{i\omega L}{V}\right)\right\}\mathfrak{I}(w_G(t))\right) + \mathbf{B}_{ac}\{\delta_{1m2}\}, \\ \mathbf{y}_{ae} = \mathbf{C}_{ae}\mathbf{x}_{ae} + \mathbf{D}_{ae}\mathbf{u}_{ae} + \mathbf{D}_{aw}\mathfrak{I}^{-1}\left(\left\{\mathbf{Q}_{HG}\left(\frac{i\omega L}{V}\right)\right\}\mathfrak{I}(w_G(t))\right) + \mathbf{D}_{ac}\{\delta_{1m2}\} \end{cases}. \qquad (A.13)$$

(4) For $\theta_{LEO} < -\delta_{LEO}$ and $\theta_{TEO} > \delta_{TEO}$:

$$\begin{cases} \dot{\mathbf{x}}_{ae} = \mathbf{A}_{ae}\mathbf{x}_{ae} + \mathbf{B}_{ae}\mathbf{u}_{ae} + \mathbf{B}_{aw}\mathfrak{I}^{-1}\left(\left\{\mathbf{Q}_{HG}\left(\frac{i\omega L}{V}\right)\right\}\mathfrak{I}(w_G(t))\right) + \mathbf{B}_{ac}\{-\delta_{1m2}\}, \\ \mathbf{y}_{ae} = \mathbf{C}_{ae}\mathbf{x}_{ae} + \mathbf{D}_{ae}\mathbf{u}_{ae} + \mathbf{D}_{aw}\mathfrak{I}^{-1}\left(\left\{\mathbf{Q}_{HG}\left(\frac{i\omega L}{V}\right)\right\}\mathfrak{I}(w_G(t))\right) + \mathbf{D}_{ac}\{-\delta_{1m2}\} \end{cases}. \qquad (A.14)$$

(5) For $\theta_{LEO} > \delta_{LEO}$ and $-\delta_{TEO} \leq \theta_{TEO} \leq \delta_{TEO}$:

$$\begin{cases} \dot{\mathbf{x}}_{ae} = \mathbf{A}_{ae}\mathbf{x}_{ae} + \mathbf{B}_{ae}\mathbf{u}_{ae} + \mathbf{B}_{aw}\mathfrak{I}^{-1}\left(\left\{\mathbf{Q}_{HG}\left(\frac{i\omega L}{V}\right)\right\}\mathfrak{I}(w_G(t))\right) + \mathbf{B}_{ac}\{\delta_{f_{LEO}}\}, \\ \mathbf{y}_{ae} = \mathbf{C}_{ae}\mathbf{x}_{ae} + \mathbf{D}_{ae}\mathbf{u}_{ae} + \mathbf{D}_{aw}\mathfrak{I}^{-1}\left(\left\{\mathbf{Q}_{HG}\left(\frac{i\omega L}{V}\right)\right\}\mathfrak{I}(w_G(t))\right) + \mathbf{D}_{ac}\{\delta_{f_{LEO}}\}, \end{cases} \qquad (A.15)$$

where

$$\mathbf{A}_{ae} = \begin{bmatrix} \mathbf{0} & \mathbf{I} & \mathbf{0} \\ -\overline{\mathbf{M}}_{HH}^{-1}(\mathbf{K}_{HHT} - q_d\mathbf{A}_{s_0}) & -\overline{\mathbf{M}}_{HH}^{-1}(\mathbf{C}_{HH} - q_d\frac{b}{V}\mathbf{A}_{s_1}) & q_d\overline{\mathbf{M}}_{HH}^{-1}\mathbf{D} \\ \mathbf{0} & \mathbf{E}_s & \frac{V}{b}\mathbf{R} \end{bmatrix}, \quad \mathbf{B}_{ac} = \begin{bmatrix} 0 \\ \overline{\mathbf{M}}_{HH}^{-1}\mathbf{\Phi}_f^T \\ 0 \end{bmatrix}[\mathbf{K}_{NM} - \mathbf{K}_L].$$

(6) For $\theta_{LEO} < -\delta_{LEO}$ and $-\delta_{TEO} \leq \theta_{TEO} \leq \delta_{TEO}$:

$$\begin{cases} \dot{\mathbf{x}}_{ae} = \mathbf{A}_{ae}\mathbf{x}_{ae} + \mathbf{B}_{ae}\mathbf{u}_{ae} + \mathbf{B}_{aw}\mathfrak{I}^{-1}\left(\left\{\mathbf{Q}_{HG}\left(\frac{i\omega L}{V}\right)\right\}\mathfrak{I}(w_G(t))\right) + \mathbf{B}_{ac}\{-\delta_{f_{LEO}}\}, \\ \mathbf{y}_{ae} = \mathbf{C}_{ae}\mathbf{x}_{ae} + \mathbf{D}_{ae}\mathbf{u}_{ae} + \mathbf{D}_{aw}\mathfrak{I}^{-1}\left(\left\{\mathbf{Q}_{HG}\left(\frac{i\omega L}{V}\right)\right\}\mathfrak{I}(w_G(t))\right) + \mathbf{D}_{ac}\{-\delta_{f_{LEO}}\}, \end{cases} \qquad (A.16)$$

where

$$\mathbf{A}_{ae} = \begin{bmatrix} \mathbf{0} & \mathbf{I} & \mathbf{0} \\ -\overline{\mathbf{M}}_{HH}^{-1}(\mathbf{K}_{HHT} - q_d\mathbf{A}_{s_0}) & -\overline{\mathbf{M}}_{HH}^{-1}(\mathbf{C}_{HH} - q_d\frac{b}{V}\mathbf{A}_{s_1}) & q_d\overline{\mathbf{M}}_{HH}^{-1}\mathbf{D} \\ \mathbf{0} & \mathbf{E}_s & \frac{V}{b}\mathbf{R} \end{bmatrix}, \mathbf{B}_{ac} = \begin{bmatrix} 0 \\ \overline{\mathbf{M}}_{HH}^{-1}\mathbf{\Phi}_f^T \\ 0 \end{bmatrix}[\mathbf{K}_{NM} - \mathbf{K}_L].$$

(7) For $-\delta_{LEO} \leq \theta_{LEO} \leq \delta_{LEO}$ and $\theta_{TEO} > \delta_{TEO}$:

$$\begin{cases} \dot{\mathbf{x}}_{ae} = \mathbf{A}_{ae}\mathbf{x}_{ae} + \mathbf{B}_{ae}\mathbf{u}_{ae} + \mathbf{B}_{aw}\mathfrak{I}^{-1}\left(\left\{\mathbf{Q}_{HG}\left(\frac{i\omega L}{V}\right)\right\}\mathfrak{I}(w_G(t))\right) + \mathbf{B}_{ac}\{\delta_{f_{TEO}}\}, \\ \mathbf{y}_{ae} = \mathbf{C}_{ae}\mathbf{x}_{ae} + \mathbf{D}_{ae}\mathbf{u}_{ae} + \mathbf{D}_{aw}\mathfrak{I}^{-1}\left(\left\{\mathbf{Q}_{HG}\left(\frac{i\omega L}{V}\right)\right\}\mathfrak{I}(w_G(t))\right) + \mathbf{D}_{ac}\{\delta_{f_{TEO}}\}, \end{cases} \qquad (A.17)$$

where

$$\mathbf{A}_{ae} = \begin{bmatrix} \mathbf{0} & \mathbf{I} & \mathbf{0} \\ -\overline{\mathbf{M}}_{HH}^{-1}(\mathbf{K}_{HHL} - q_d\mathbf{A}_{s_0}) & -\overline{\mathbf{M}}_{HH}^{-1}(\mathbf{C}_{HH} - q_d\frac{b}{V}\mathbf{A}_{s_1}) & q_d\overline{\mathbf{M}}_{HH}^{-1}\mathbf{D} \\ \mathbf{0} & \mathbf{E}_s & \frac{V}{b}\mathbf{R} \end{bmatrix}, \mathbf{B}_{ac} = \begin{bmatrix} 0 \\ \overline{\mathbf{M}}_{HH}^{-1}\mathbf{\Phi}_f^T \\ 0 \end{bmatrix}[\mathbf{K}_{NM} - \mathbf{K}_T].$$

(8) For $-\delta_{LEO} \leq \theta_{LEO} \leq \delta_{LEO}$ and $\theta_{TEO} < -\delta_{TEO}$:

$$\begin{cases} \dot{\mathbf{x}}_{ae} = \mathbf{A}_{ae}\mathbf{x}_{ae} + \mathbf{B}_{ae}\mathbf{u}_{ae} + \mathbf{B}_{aw}\mathfrak{I}^{-1}\left(\left\{\mathbf{Q}_{HG}\left(\frac{i\omega L}{V}\right)\right\}\mathfrak{I}(w_G(t))\right) + \mathbf{B}_{ac}\{-\delta_{f_{TEO}}\}, \\ \mathbf{y}_{ae} = \mathbf{C}_{ae}\mathbf{x}_{ae} + \mathbf{D}_{ae}\mathbf{u}_{ae} + \mathbf{D}_{aw}\mathfrak{I}^{-1}\left(\left\{\mathbf{Q}_{HG}\left(\frac{i\omega L}{V}\right)\right\}\mathfrak{I}(w_G(t))\right) + \mathbf{D}_{ac}\{-\delta_{f_{TEO}}\}, \end{cases} \qquad (A.18)$$

where

$$\mathbf{A}_{ae} = \begin{bmatrix} \mathbf{0} & \mathbf{I} & \mathbf{0} \\ -\overline{\mathbf{M}}_{HH}^{-1}(\mathbf{K}_{HHL}-q_d\mathbf{A}_{s_0}) & -\overline{\mathbf{M}}_{HH}^{-1}(\mathbf{C}_{HH}-q_d\frac{b}{V}\mathbf{A}_{s_1}) & q_d\overline{\mathbf{M}}_{HH}^{-1}\mathbf{D} \\ \mathbf{0} & \mathbf{E}_s & \frac{V}{b}\mathbf{R} \end{bmatrix}, \mathbf{B}_{ac} = \begin{bmatrix} 0 \\ \overline{\mathbf{M}}_{HH}^{-1}\boldsymbol{\Phi}_f^T \\ 0 \end{bmatrix}[\mathbf{K}_{NM}-\mathbf{K}_T].$$

(9) For $-\delta_{LEO}\le\theta_{LEO}\le\delta_{LEO}$ and $-\delta_{TEO}\le\theta_{TEO}\le\delta_{TEO}$:

$$\begin{cases} \dot{\mathbf{x}}_{ae} = \mathbf{A}_{ae}\mathbf{x}_{ae} + \mathbf{B}_{ae}\mathbf{u}_{ae} + \mathbf{B}_{aw}\mathfrak{I}^{-1}\left(\left\{\mathbf{Q}_{HG}\left(\frac{i\omega L}{V}\right)\right\}\mathfrak{I}(w_G(t))\right), \\ \mathbf{y}_{ae} = \mathbf{C}_{ae}\mathbf{x}_{ae} + \mathbf{D}_{ae}\mathbf{u}_{ae} + \mathbf{D}_{aw}\mathfrak{I}^{-1}\left(\left\{\mathbf{Q}_{HG}\left(\frac{i\omega L}{V}\right)\right\}\mathfrak{I}(w_G(t))\right), \end{cases} \tag{A.19}$$

where

$$\mathbf{A}_{ae} = \begin{bmatrix} \mathbf{0} & \mathbf{I} & \mathbf{0} \\ -\overline{\mathbf{M}}_{HH}^{-1}(\mathbf{K}_{HHLT}-q_d\mathbf{A}_{s_0}) & -\overline{\mathbf{M}}_{HH}^{-1}(\mathbf{C}_{HH}-q_d\frac{b}{V}\mathbf{A}_{s_1}) & q_d\overline{\mathbf{M}}_{HH}^{-1}\mathbf{D} \\ \mathbf{0} & \mathbf{E}_s & \frac{V}{b}\mathbf{R} \end{bmatrix}.$$

References

Albano, E., Rodden, W.P., 1969. A doublet-lattice method for calculating lift distributions on oscillating surfaces in subsonic flows. AIAA Journal 7 (2), 279–285.

Anderson, W.D., Mortara, S., 2007. Maximum control surface freeplay, design and flight testing approach on the F-22. AIAA Paper. (2007-1767).

Bae, J.S., 2002. Aeroelastic Characteristics and Flutter Suppression Considering Structural Nonlinearity. Ph.D. Dissertation, Department of Aerospace Engineering. Korea Advanced Institute of Science Technology.

Bae, J.S., Yang, S.M., Lee, I., 2002. Linear and nonlinear aeroelastic analysis of fighter-type wing with control surface. Journal of Aircraft 39 (4), 697–708.

Bae, J.S., Inman, D.J., Lee, I., 2004. Effects of structural nonlinearities on subsonic aeroelastic characteristics of an aircraft wing with control surface. Journal of Fluids and Structures 19, 747–763.

Chen, Y.M., Liu, J.K., Meng, G., 2011. Equivalent damping of aeroelastic system of an airfoil with cubic stiffness. Journal of Fluids and Structures 27, 1447–1454.

Chung, K.W., Chan, C.L., Lee, B.H.K., 2007. Bifurcation analysis of a two-degree-of-freedom aeroelastic system with freeplay structural nonlinearity by a perturbation-incremental method. Journal of Sound and Vibration 299, 520–539.

Conner, M.D., Tang, D.M., Dowell, E.H., Virgin, L.N., 1997. Nonlinear behavior of a typical airfoil section with control Surface freeplay: a numerical and experimental Study. Journal of Fluids and Structures 11, 89–109.

Cui, P., Han, J.L., 2011. Numerical investigation of the effects of structural geometric and material nonlinearities on limit-cycle oscillation. Journal of Fluids and Structures 27, 611–622.

Dimitriadis, G., Cooper, J.E., 2000. Characterization of the behaviour of a simple aeroservoelastic system with control nonlinearities. Journal of Fluids and Structures 14, 1173–1193.

Dowell, E.H., Tang, D.M., 2002. Nonlinear aeroelasticity and unsteady aerodynamics. AIAA Journal 40, 1697–1707.

Dowell, E.H., Thomas, J.P., Hall, K.C., 2003. Transonic limit cycle oscillation analysis using reduced order aerodynamic models. Journal of Fluids and Structures 19, 17–27.

Firouz-Abadi, R.D., Alavi, S.M., Salarieh, H., 2013. Analysis of non-linear aeroelastic response of a supersonic thick fin with plunging, pinching and flapping free-plays. Journal of Fluids and Structures 40, 163–184.

Frampton, K.D., Clark, R.L., 2000. Experiments on control of limit-cycle oscillations in a typical section. Journal of Guidance, Control and Dynamics 23, 956–960.

Gold, P., Karpel, M., 2008. Reduced-size aeroservoelastic modeling and limit-cycle-oscillation simulations with structurally nonlinear actuators. Journal of Aircraft 45 (2), 471–477.

Gordon, J.T., Meyer, E.E., Minogue, R.L., 2008. Nonlinear stability analysis of control surface flutter with free-play effects. Journal of Aircraft 45 (6), 1904–1916.

Huang, Y., Hu, D.L., Liu, X.B., 2012. Center manifold reduction for the flutter of airfoils with gust loading. Journal of Fluids and Structures 30, 133–140.

Jones, D.P., Roberts, I., Gaitonde, A.L., 2007. Identification of limit cycles for piecewise nonlinear aeroelastic systems. Journal of Fluids and Structures 23, 1012–1028.

Karpel, M., Moulin, B., Chen, P.C., 2005. Dynamic response of aeroservoelastic systems to gust excitation. Journal of Aircraft 42 (5), 1264–1272.

Karpel, M., Raveh, D., 1996. Fictitious mass element in structural dynamics. AIAA Journal 34 (3), 607–613.

Kim, J.Y., Kim, K.S., Lee, I., 2008. Transonic aeroelastic analysis of all-movable wing with free play and viscous effects. Journal of Aircraft 45 (5), 1820–1824.

Lee, D.H., Chen, P.C., 2006. Nonlinear aeroelastic studies on a folding wing configuration with free-play hinge nonlinearity. AIAA Paper. (2006-1734).

Lee, I., Kim, S.H., 1995. Aeroelastic analysis of a flexible control surface with structural nonlinearity. Journal of Aircraft 32 (4), 868–874.

Liu, L., Wong, Y.S., Lee, B.H.K., 2002. Nonlinear aeroelastic analysis using the point transformation method, part 1: freeplay model. Journal of Sound and Vibration 253 (2), 447–469.

Marsden, C.C., Price, S.J., 2005. The aeroelastic response of a wing section with a structural freeplay nonlinearity: an experimental investigation. Journal of Fluids and Structures 21, 257–276.

Mukhopadhyay, V., 1990. Control Law Synthesis and Stability Margin Improvement Using Constrained Optimization, Advances in Aerospace Systems Dynamics and Control Systems, Theory and ApplicationsAcademic Press, New York163–204.

Mukhopadhyay, V., Newsom, J.R., Abel, I., 1982. Reduced-order optimal feedback control law synthesis for flutter suppression. Journal of Guidance, Control and Dynamics 5 (4), 389–395.

Seo, Y.J., Lee, S.J., Bae, J.S., Lee, I., 2011. Effects of multiple structural nonlinearities on limit cycle oscillation of missile control fin. Journal of Fluids and Structures 27, 623–635.

Shin, W.H., Lee, S.J., Lee, I., Bae, J.S., 2007. Effects of actuator nonlinearity on aeroelastic characteristics of a control fin. Journal of Fluids and Structures 23, 1093–1105.

Stanford, B., Beran, P., 2013. Direct flutter and limit cycle computations of highly flexible wings for efficient analysis and optimization. Journal of Fluids and Structures 36, 111–123.

Tang, D.M., Dowell, E.H., Virgin, L.N., 1998. Limit cycle behavior of an airfoil with a control surface. Journal of Fluids and Structures 12 (7), 839–858.

Vasconcellos, R., Abdelkefi, A., Marques, F.D., Hajj, M.R., 2012. Representation and analysis of control surface freeplay nonlinearity. Journal of Fluids and Structures 31, 79–91.